ACADÉMIE
DES SCIENCES
INSTITUT DE FRANCE

Comptes Rendus

Géoscience

Sciences de la Planète

Loic Labrousse, Guillaume Bonnet, Camille François, Antoine Godet and Thomas Gyomlai

Recent advances in petrochronology: from dates to ages and rates of deep orogenic processes

Volume 356, Special Issue S2 (2024), p. 551-577

Online since: 4 April 2024

Part of Special Issue: Geodynamics of Continents and Oceans – A tribute to Jean Aubouin

Guest editors: Olivier Fabbri (Université de Franche-Comté, UMR CNRS 6249, Besançon), Michel Faure (Université d'Orléans-BRGM, UMR CNRS 7325, Institut des Sciences de la Terre, Orléans), Jacky Ferrière (Université de Lille, faculté des Sciences), Laurent Jolivet (Sorbonne Université, ISTeP, UMR 7193, Paris) and Sylvie Leroy (Sorbonne Université, CNRS-INSU, ISTeP, Paris)

https://doi.org/10.5802/crgeos.234

The Comptes Rendus. Géoscience — Sciences de la Planète *are a member of the Mersenne Center for open scientific publishing*
www.centre-mersenne.org — e-ISSN : 1778-7025

ACADÉMIE DES SCIENCES
INSTITUT DE FRANCE

Comptes Rendus. Géoscience — Sciences de la Planète
2024, Vol. 356, Special issue S2, p. 551-577
https://doi.org/10.5802/crgeos.234

Review article

Geodynamics of Continents and Oceans – A tribute to Jean Aubouin

Recent advances in petrochronology: from dates to ages and rates of deep orogenic processes

Loic Labrousse[*,a], **Guillaume Bonnet**[a], **Camille François**[a,b], **Antoine Godet**[c,d] **and Thomas Gyomlai**[a]

[a] Sorbonne Université, CNRS-INSU, Institut des Sciences de la Terre Paris, ISTeP UMR 7193, F-75005 Paris, France

[b] Commission de la Carte Géologique du Monde, 77 rue Claude Bernard, 75005 Paris, France

[c] E4M, Département de géologie et de génie géologique, Université Laval, Québec, Canada

[d] Natural Resources Canada, Geological Survey of Canada, 490 rue de la Couronne, Québec (Québec), G1K 9A9, Canada

E-mails: loic.labrousse@sorbonne-universite.fr (L. Labrousse), gbonnet01@gmail.com (G. Bonnet), francois.camille555@gmail.com (C. François), antoine.godet.1@ulaval.ca (A. Godet), thomas.gyomlai@sorbonne-universite.fr (T. Gyomlai)

Abstract. In order to decipher the prevalent processes active at depth in orogenic systems, their time sequence and their rates have to be assessed. This is essentially done via absolute dating of accessory and rock-forming metamorphic minerals. The interpretation of dates, now produced in high quantities and low uncertainties, with geochemical and textural information thanks to *in situ* dating techniques, into ages with a geological meaning, is based on sophisticated multi-disciplinary approaches. The wealth of data produced during the last decades in internal zones of mountain chains today questions some of the seminal concepts in geodynamics as well as in petrochronology. The concept of closure temperature Jäger [1967] but also the notions of metamorphic unit or metamorphic event are now to be considered in the light of campaign-style dating projects, that enable a comprehensive and statistical interpretation of age patterns from the mineral scale to the geodynamic process scale.

Keywords. Petrochronology, Tectonics, Metamorphism.

Manuscript received 20 April 2023, accepted 6 September 2023.

1. Introduction

The developments of geochronology and tectonics have numerous intrications. The advent of modern geochronology is associated with the improvements in mass spectrometry in the 1930s and 1940s, but the earliest published dates are older, including measurements of elemental lead in uranium-rich minerals by Holmes [1911], in what is considered as the first geochronology paper [in Davis et al., 2003]. Interestingly, the first U–Pb age review was published by Barrell [1917] so that the two first geologists basing their understanding on geochronology data were Holmes, who linked continental drift to mantle convection Holmes [1928], and Barrell, who elaborated

[*] Corresponding author

the notion of lithosphere in the seminal "Strength of the Earth" paper series Barrell [1914]. So deep tectonics and high temperature geochronology actually share the same genealogy.

In the early 1960's the first understanding of the link between metamorphic series and orogeny, i.e. the enunciation of metamorphic gradients Miyashiro [1961], is partly based on K–Ar ages. The application of radiochronology to the internal zones of mountain belts was also immediate with the seminal K–Ar and Rb–Sr ages by Emilie Jäger and coworkers Jäger et al. [1961], Jäger [1962] on the Simplo-Ticinese high temperature metamorphic dome, which could be considered as the cradle of metamorphic dating. K–Ar or Rb–Sr ages produced had 2 to 3 Myr uncertainties for 18 to 20 Ma absolute values, i.e. 5 to 15% relative precision. This allowed the systematic discrepancy of K–Ar or Rb–Sr ages yielded by biotite and muscovite to be brought out in the very same decade Armstrong et al. [1966], at the same time tools were developed to assess the statistical significance of the produced ages [with the MSWD parameter for instance, York, 1966].

Based on the notion of closure temperature of Jäger [1967], Dodson [1973] formulates the effect of temperature and diffusion on isotope concentrations and sets the first framework used for interpreting radiometric data: crystallization or cooling ages. We may try to elaborate on the present-day difficult emancipation from this framework.

A decisive stage to mention along these 60 years is the advent of *in situ* dating, with the elaboration of secondary ion mass spectrometry (SIMS) and sensitive high-resolution ion microprobe (SHRIMP), the laser ablation–inductively coupled plasma–mass spectrometry (LA-ICP-MS) techniques and recent development of collision–reaction cell mass spectrometers allowing to resolve the isobaric interferences. While the time-consuming isotopic dilution–thermal ionization mass spectroscopy (ID-TIMS), tuned by Tilton et al. [1955], still has the highest age resolution with less than 0.1% 2σ precision and accuracy Schaltegger et al. [2015], SIMS and SHRIMP, developed in the 70's and 80's respectively, yield *in situ* dating of 10 to 30 μm diameter domains with a shallow pit depth and a precision now below 3% Schoene [2014]. LA-ICP-MS, the easiest method to set up, most of the time requires larger analytical volumes (up to 100 μm spots, with depth about the same order) and yields ages with a 3% resolution in the shortest analytical time Schaltegger et al. [2015].

The present contribution does not have the pretention to add to the list of extensive petrochronology reviews Kohn et al. [2017], Kohn [2016], Kylander-Clark et al. [2013], Schoene [2014] but rather proposes to elaborate on how the use of radiometric ages in metamorphic petrology is currently changing from pinning PT paths in time to assessing duration of processes (i.e. metamorphism and deformation) and hence their characteristic time-scale and rates, and eventually associating *in situ* dating and strain analysis at the mineral scale rather than adding ages along of a PT-strain path. This approach actually fits into the larger definition of petrochronology "*the branch of Earth science that is based on the study of rock samples and that links time (i.e., ages or duration) with specific rock-forming processes and their physical conditions*" Engi et al. [2017]. The scope of the present review is restricted to regional metamorphism, from HP to UHP conditions and UHT conditions, down to greenschist facies. The latest stages of exhumation through lower temperatures, mainly documented through thermochronology studies will not be elaborated on here.

The classical approach remains two-fold depending on whether the datable mineral is a major rock-forming mineral or an accessory phase, whose paragenetic significance is not explicit. *In situ* dating of radioactive accessory minerals is now extremely precise but requires the obtained "dates", i.e. the numerical values deduced from isotopic and elemental ratios measures Schoene [2014] to be mutually correlated and linked to index minerals for their interpretation as a meaningful metamorphic "age". The second approach based on the direct dating of rock-forming minerals involves K–Ar, Rb–Sr, Sm–Nd or Lu–Hf radiogenic systems, on ubiquitous silicates such as mica or garnet. The principal issue is then the significance of the dates obtained, in terms of crystallization, strain or cooling age for instance.

A new landscape is now emerging with on one side the use of more sophisticated chemical systems including U-rich minerals such as rutile, allanite or even epidote in equilibrium assemblages, blurring the limit between major and accessory phases, and on the other side the lowering of analytical sensitivity allowing to date practically any mineral [U–Pb on garnet, Millonig et al., 2020, Rb–Sr on illite and

adularia in ancient faults, Tillberg et al., 2020, or U–Pb on calcite from faults, see Lacombe and Beaudoin, 2024, this volume], so that the alternative expressed above is fading.

On the other side, the better understanding of diffusion processes and the confrontation of experimentally determined diffusion coefficient to natural data or modelling of effective diffusion of ions through crystal lattices also challenges the orthodoxy of the Dodson alternative: crystallize or cool. The role of fluids and strain in the opening of minerals to isotopic and elemental fluxes is now well documented.

The richness of the present-day toolbox is best expressed in the "multi-tool" and "campaign-styles" approaches that now question the significance of tectonic units in time and space. The advent of microstructural geochronology Moser et al. [2017] with the use of TEM and atomic probe tomography (APT) that combines imaging with elemental and isotopic composition measurement at the nanometer scale, is perhaps the next break-through in high temperature geochronology as it directly images how crystalline defects control isotope concentrations, and hence how strain can be dated.

2. Two strategies to pin ages along PT paths

2.1. *Ages from accessory minerals*

2.1.1. *Based on textures*

The strongest textural evidence used in the relative dating of accessory and rock-forming phases remains the host-inclusion relationship, the datable mineral being itself included or bearing inclusions. The most reliable dating of Ultra-High Pressure (UHP) metamorphic peaks, for instance, is based on this principle: an inclusion of coesite in dated zircon grains, evidences that these grew in the coesite stability field. Even though diamond-hosting zircons were dated in the Kokchetav massif as early as 2001 Hermann et al. [2001], the case of zircon from the Caledonian UHP province of Northeast Greenland [NEGEP, North East Greenland Eclogite Province, Gilotti, 1993] is perhaps the one that had the most critical impact on the understanding of UHP metamorphism tectonic significance. Dating of zircon grains hosting inclusions symptomatic of UHP eclogite facies (e.g. garnet, omphacite, and coesite, Figure 1A has demonstrated that the NEGEP UHP episode occurred in the Carboniferous [356–350 Ma, McClelland et al., 2006], i.e. late in the Caledonian collision sequence. The thermo-mechanical implications of such a late UHP stage for collision dynamics is not fully understood yet Gilotti and McClelland [2007]. The inclusion of datable minerals in rock-forming minerals also offers the potential to date their growth. Among decisive studies in this prospect, the extensive dating of monazite grains in inclusion in garnet from an upper amphibolite facies pelitic schist from the Grouse Creek Mountains (Northwest Utah, USA) is often cited Hoisch et al. [2008]. The age of monazite grains constitutes an upper bound for the age of the garnet growth itself [Kohn, 2016, Figure 1B].

2.1.2. *Based on trace elements fingerprinting*

In situ Rare Earth Elements (REE) signature of zircon domains can be produced by LA-ICP-MS and/or SHRIMP analysis Schaltegger et al. [1999], Rubatto [2002]. Such data is now routinely obtained together with ages on zircon, but also monazite or titanite with Split Stream (LASS)-ICP-MS [Kylander-Clark et al., 2013, Figure 2A]. The slope of the REE signature in the HREE (Heavy Rare Earth Elements) domain and the absence/presence of a Europium anomaly (Eu/Eu*) are among the most widely used criteria. A depletion in the HREE domain is generally consistent with a growth episode in the garnet stability field while the depletion in Eu suggests growth in equilibrium with a Ca-bearing phase such as plagioclase. Although the effect of bulk rock composition, growth and breakdown of major and other accessory phases, the presence of melt [Figure 2B,C, Walczak et al., 2022, Pitra et al., 2022] or the oxygen fugacity Kohn [2016] may alter these trends, they remain an effective tool for the interpretation of calculated dates in zircon Rubatto [2017] as well as in monazite [Foster et al., 2002, Holder et al., 2015, Larson et al., 2022, for instance]. Nevertheless, growth of zircon, or monazite, considered at the equilibrium with existing garnet, or plagioclase, does not imply coeval growth of both major and accessory minerals Kohn [2016], Pitra et al. [2022].

2.1.3. *Based on 4+ cations thermometry*

Titanium substitutes for Si in zircon, while Zr substitutes for Ti in rutile and titanite Zack et al. [2004],

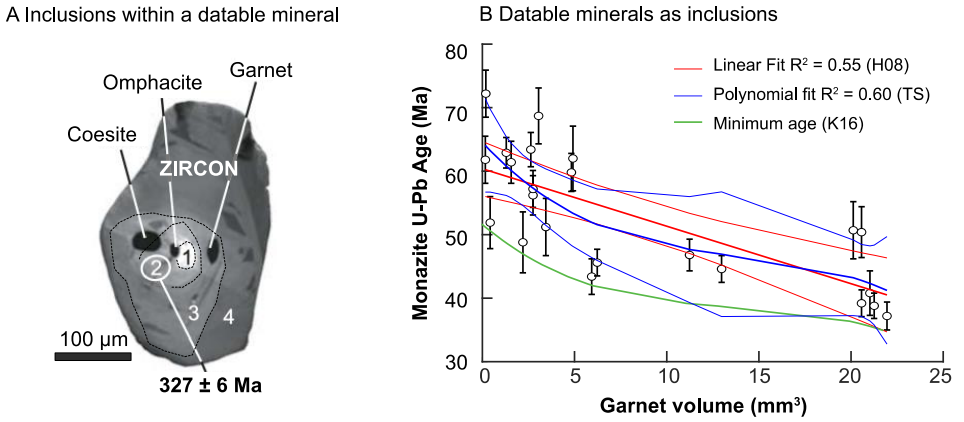

Figure 1. Inclusion relationships between datable and index minerals. (A) UHP Eclogite facies paragenesis as inclusions in a zircon core from the North Eastern Greenland Eclogite Province. SHRIMP dating spot in coesite-bearing zone 2 yields 357 ± 6 Ma for the UHP stage [modified after McClelland et al., 2006]. (B) U–Pb ages of monazite inclusions depending on their structural position in garnet volume (as their radial position cubed). Data from Hoisch et al. [2008]. In red: linear interpolation, as in Hoisch et al. [2008]; in green maximum age curve for garnet growth, as in Kohn, 2016; in blue: polynomial interpolation.

Kohn [2020]. These substitutions have been calibrated in temperature over the whole metamorphic range (400 °C–1000 °C) at fixed and varied pressures and yield T estimates with uncertainties lower than ±25 °C Watson et al. [2006], Tomkins et al. [2007], Hayden et al. [2008]. Zr-in-rutile and Ti-in-zircon methods are actually based on cation exchanges assuming that quartz, rutile and zircon are costable (i.e. with activities = 1). Corrections should be applied when the SiO_2 activity is lower than 1 or for instance when the peak temperature is known to lie in the coesite field Kohn [2020]. Based on the similarly low diffusivities of Pb and Ti in zircon, the Ti-in-zircon thermometry is expected to yield the crystallization condition of the dated zircon domain. Zirconium-in-rutile thermometry is also expected to yield equilibration at peak temperature, although some cases of relict cores with preserved prograde temperatures or incomplete equilibration cases due to shielding or slow diffusion at the aggregate scale have been described for rutile Kohn [2020].

2.2. *Ages from rock-forming minerals*

2.2.1. *Pinning dates along the crystal growth history*

Among metamorphic rock-forming minerals, mica and garnet are perhaps the most popular for dating. In the past 20 years, the ^{39}Ar–^{40}Ar radiometric method has been predominantly used to date mica, by opposition to Rb–Sr, until recently not accessible *in situ* and still hampered by the availability of homogeneous standard materials Jegal et al. [2022]. However, in recent years, the addition of a reaction cell between the quadrupoles in the MS device has enabled the use of reacting gases of various reaction affinities with isobaric elements to resolve isobaric interferences at $m = 87$. In the case of mica, this allows to separate ^{87}Sr and ^{87}Rb and enables *in situ* Rb–Sr dating [with O_2, NO_2 or NH_3 as reacting gases, Zack and Hogmalm, 2016, Hogmalm et al., 2017]. The obtained biotite-only isochrons are based on a large amount of data points that compensates for their large uncertainties, adds a textural control, and requires simpler processing compared to the ID-TIMS approach (Figure 3).

In garnet, the comparison of Lu–Hf and Sm–Nd ages yielded by ID-MC-ICP-MS or TIMS analysis on whole-rock and garnet fractions from the same rocks shows recurrent older Lu–Hf ages and younger Sm–Nd ages Ibañez-Mejia et al. [2018], Baxter et al. [2017], Johnson et al. [2018]. This has been assigned to different closure temperatures, different diffusion rates and different partition coefficients. Thus, at constant grain size and cooling rates, the Sm–Nd isotopic

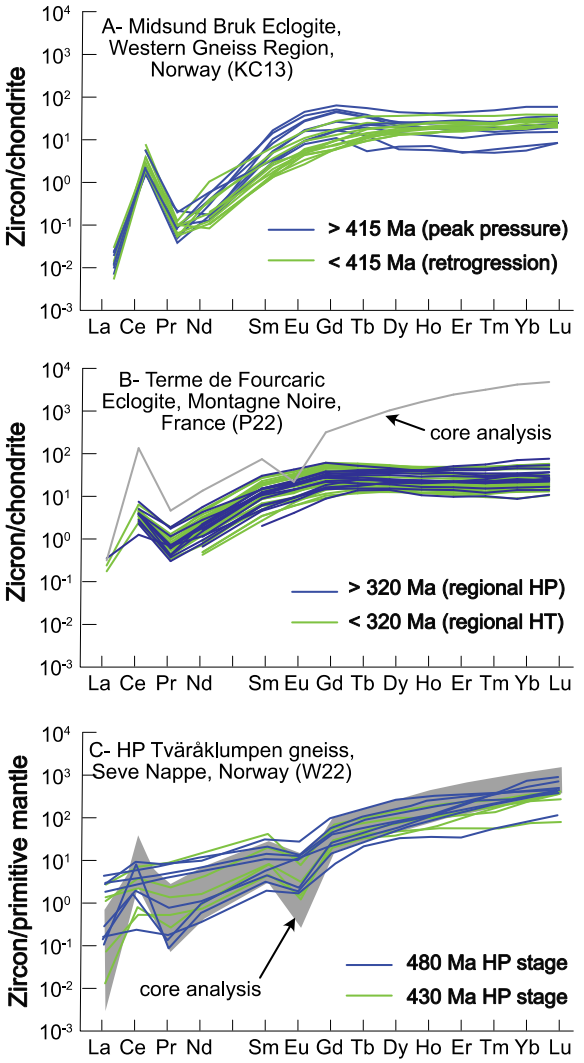

Figure 2. Rare Earth Elements spectra of eclogite-facies and retrogression-related zircons showing different behaviors. (A) Western Gneiss Region, Norway [data from Kylander-Clark et al., 2013] Pressure peak zircons with ages above 415 Ma show negative slope spectra in the HREE domain while younger zircons associated to retrogression show positive slope. (B) Montagne Noire, France [data from Pitra et al., 2022]: Both old (>320 Ma, associated to regional HP stage) and young (<320 Ma, associated to regional partial melting) zircons appear depleted in the HREE domain, (C) Seve Nappe, Swedish Caledonides [data from Walczak et al., 2022] Two successive HP stages zircon populations show REE spectra similar to inherited zircon cores.

system has a lower closure temperature (<700 °C) compared to Lu–Hf [>750 °C e.g. Scherer et al., 2001, Smit et al., 2013]. Diffusive exchange with the matrix also plays a role, as a net loss or gain of parent isotopes may influence the chronometer systematics [e.g. Bloch and Ganguly, 2015]. A significant Rayleigh fractionation for lutetium also yields Lu–Hf ages to be weighted towards the timing of garnet core crystallization, while the Sm–Nd method yields ages representative of the average grain growth [Smit et al., 2013, Lotout et al., 2018, for instance] or homogenization at HT peak conditions. By trying to link garnet age to prograde metamorphic reactions, fine analyses [e.g. Konrad-Schmolke et al., 2008, Godet et al., 2020b] have shown that the early uptake in Lu during prograde growth of garnet could actually relate to the breakdown of Lu-rich low-grade minerals such as chlorite. Lu–Hf dating of garnet for a mafic protolith could therefore approximate the crossing time of the chlorite-out garnet-in reaction, while Sm–Nd age could relate to the successive epidote or amphibole-out reactions occurring along a burial sequence Baxter et al. [2017].

While new alternatives to mechanical microsampling have emerged, based for instance on laser ablation coupled with ID-TIMS analysis Logue et al. [2022] or MC-ICP-MS Tual et al. [2022] on smaller and smaller texturally selected domains in rocks, *in situ* dating of garnet using triple quadrupole LA-ICP-MS technique appears to be a promising alternative. The setup of the triple quadrupole LA-ICP-MS allows to resolve the mass interference at 176 amu between Lu, Hf and Yb [with NH_3 as a reacting gas, Simpson et al., 2021] and enables *in situ* Lu–Hf dating.

2.2.2. *Challenging the closure temperature paradigm*

The closure temperature concept Jäger [1967] actually stems from the interpretation of Rb–Sr and K–Ar ages on micas from the Simplo-Ticinese high temperature metamorphic dome. The dated thermal event was considered as associated to limited strain and temperature-driven diffusion as the first order process governing the diffusion of radioactive decay products. Even though temperature was indeed a first order parameter controlling the regional age pattern, some old ages were preserved in the alpine-age domain Arnold and Jäger [1965], evidencing from the start that some processes different from thermally activated diffusion (i.e. recrystallization, fluid influx)

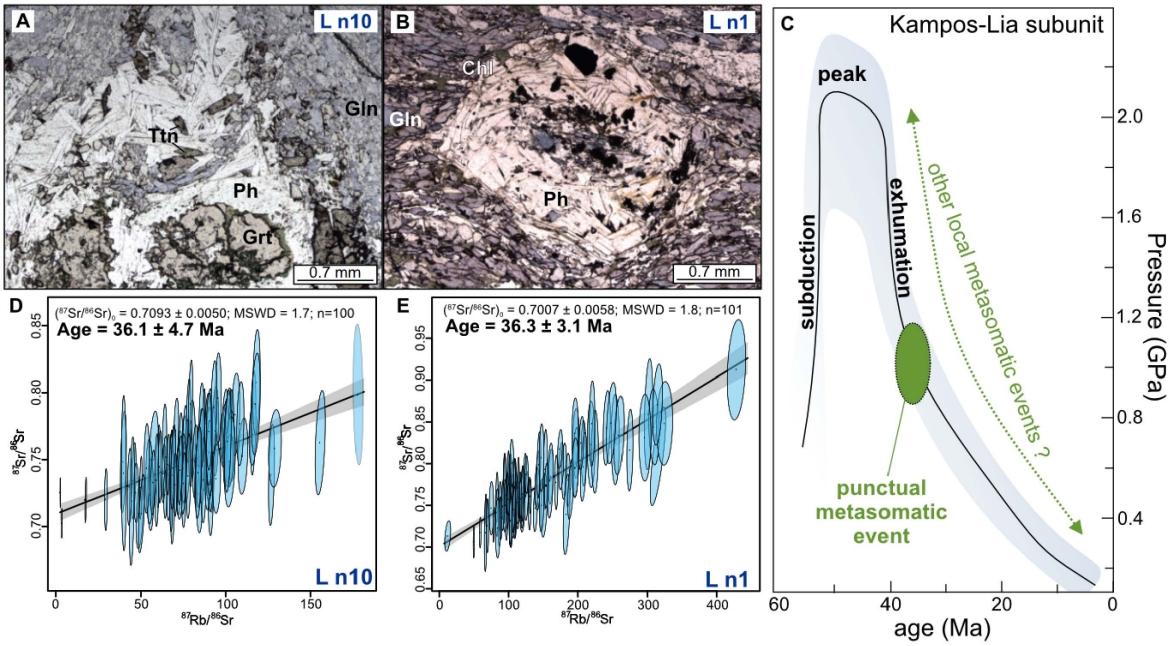

Figure 3. Example of hygrochronometry with the dating of fluid-driven crystallization of phengite, related to a metasomatic K-enrichment in metavolcanite previously devoid of mica, from the Kampos-Lia subunit in Syros, Greece. Phengite is associated with chlorite and gradually replacing garnet and provides ages around 36 Ma. Synthetic pressure–time path showing the metasomatic event, which corresponds to a punctual event occurring during exhumation of the previously subducted Kampos-Lia subunit. Modified from Gyomlai et al. [2023].

were required at the local scale to fully reset the considered chronometers Villa [1998]. The refinement of the closure temperature concept by also introducing an "opening temperature" and a "resetting temperature" along the prograde path Gardés and Montel [2009] actually makes it much more complex for age interpretation. Indeed, as these two prograde thresholds frame the closure temperature value, a complex set of combinations appears depending on the temperature interval in which the considered mineral crystallized.

Eventually the closure temperature estimates given by the Dodson equation are based on diffusion coefficients, themselves mostly deduced from experiments. The differences between experimental conditions and nature [fluid regime, crystal defects density in minerals, see Nteme et al., 2022 for discussion for Ar] seem to systematically yield minimum values for effective closure temperature in nature.

Even for minerals considered as refractory to isotope disturbance in most of the metamorphic conditions, a purely diffusive model does not explain all natural data. Monazite, for instance, is prone to decoupling between ages (i.e. U–Pb system behavior) and textures (cores vs rims) in the supra-solidus domain [$T > 800$–850 °C; Weinberg et al., 2020]. However, at odds with the phase equilibria models predicting complete dissolution above ~850 °C Kelsey et al. [2008], Yakymchuk and Brown [2014], subsolidus prograde monazite might still preserve their age in granulitic domains experiencing partial melting [e.g. Didier et al., 2015, Nicollet et al., 2018, Godet et al., 2020a].

U–Pb apatite dating, often used as a thermochronometer, can also be considered as a valuable tracker of fluid rock-interactions over the greenschist to amphibolite facies temperature interval Kirkland et al. [2018]. In the Central Alps, apatite grains from alpine upper greenschist to amphibolite facies orthogneiss preserve their hercynian ages Henrichs et al. [2019], although they reached temperatures close to or even beyond the acknowledged closure

temperature for Pb in apatite [375–550 °C, Cochrane et al., 2014]. This contrasted behavior is attributed to different fluid regimes, orthogneiss remaining relatively dry compared to their cover counterparts.

Therefore, it seems that discussing ages on the a priori basis of the closure temperature paradigm alone runs counter to the precision (both analytical and scientific) reached today, that allows a case-by-case analysis of the conditions under which an isotopic system may close. Considerations on the size of the Ar ion for instance Villa [1998], Bosse and Villa [2019] and modelling of its interactions with the crystalline framework Nteme et al. [2022] point to the conclusion that its thermal diffusion is actually less efficient in pristine crystals than estimated via experiments. Considering the closure of a mineral as the end of its interaction with the external media, through fluids, whose properties and amount relate to temperature, but also strain, rather than a direct effect of temperature is perhaps a more comprehensive paradigm. The term "hygrochronometry" Villa [2016] is sometimes used for this purpose. Identifying such fluid-driven recrystallization allows to date punctuated fluid ingression, in particular in strain-free samples, with duration below dating precision [Gyomlai et al., 2023, Figure 3].

A convincing example of how fluids, together with strain, can actually control the behavior of parageneticchronometers at the aggregate scale is given by Airaghi et al. [2018] on micaschists from the Longmen Shan belt, China, that have experienced peak metamorphic conditions of 530 °C to 580 °C. In situ ^{40}Ar–^{39}Ar dating of biotite porphyroblasts cores yielded prograde ages, significantly older than their rims, returning ages close to peak stage defined by allanite crystallization (Figure 4). White mica yielded scattered ages with 3 distinct generations, the two younger being texturally related to retrogression (Figure 4). The age difference of more than 40 Myr between biotite rims ages and white mica ages is plainly at odds with any of the estimates for closure temperature of muscovite and biotite for argon [estimated at 280 and 450 °C respectively in Airaghi et al., 2018]. However, a plausible explanation is given by the contrasting crystal habits of the two phases, the biotite porphyroblasts having been shielded from a series of resetting mechanisms, i.e. fluid-driven recrystallization and intra-grain porosity development, active in the white mica generations. White mica hence recorded several stages of fluid-influx/strain, while biotite retained its high T crystallization age.

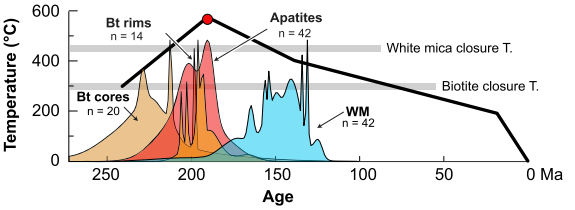

Figure 4. Temperature–time path and successive ^{39}Ar–^{40}Ar ages obtained on biotite cores and rims, apatite and white mica from the Longmen Shan micaschists [data from Airaghi et al., 2018]. Frequency curves are summed normal distribution curves for each age normalized to their maximum. White mica and biotite closure temperature values as estimated by Airaghi et al. [2018].

3. Out of the classical alternative

3.1. *Blurring the lines between accessory and rock-forming minerals*

Among accessory minerals, some show phase equilibria relationships that allow their growth/breakdown to be linked to metamorphic paragenesis and hence what is referred to as "reaction dating".

Zircon is perhaps the least-constrained datable accessory mineral in terms of reactions. Relationships with melt and supercritical fluids at high P and T have been documented Hermann et al. [2013] but also at low T, as numerous prograde ages have been assessed on basis of meticulous case-by-case analysis McClelland and Lapen [2013], Gervais and Crowley [2017], Godet et al. [2020b]. The titaniferous phases have stability fields that depend on rock chemistry, P, T, and xH_2O Engi et al. [2017], Kohn [2020]. In regular and UHP eclogite-facies assemblages, rutile is usually the stable titaniferous mineral. Bonnet et al. [2022] used this specificity in high and ultrahigh-pressure metamorphic units in the Dora-Maira Massif, Western Alps. In addition to the textural equilibrium of rutile with peak minerals, coupled rutile Zr thermometry and geochronology offers an opportunity to evaluate equilibration conditions across samples (Figure 5). The stability field

of titanite to pressure conditions < 1.5 GPa makes it a good marker of exhumation Spencer et al. [2013]. For higher temperature metamorphic rocks (peak ≥ 800 °C) the interpretation of rutile ages is more complex. For example, the oldest titanite ages in the WGR (Norway) imply that decompression under 1.5 GPa be older than 405 Ma Spencer et al. [2013], whereas rutile ages are systematically younger on a regional scale [375–400 Ma, Schärer and Labrousse, 2003, Kylander-Clark et al., 2008, Cutts et al., 2019]. Rutile ages have therefore been interpreted as early cooling ages after their crystallization as part of the eclogite facies paragenesis.

Monazite, xenotime, allanite and their possible mutual relationships have also been described in detail Janots et al. [2008], Manzotti et al. [2018]. Allanite, preserved above 450 °C in Ca-rich rocks, breaks down into monazite and xenotime above 560–610 °C in Ca-poor rocks. The incorporation of monazite and xenotime into the NCKFMASHMnPFCeY chemical system Spear and Pyle [2010] is consistent with this observation. The monazite field actually coincides with the amphibolite facies, shifted towards greenschists, resp. granulites, if the Ca content of the rock is particularly low, resp. high Schulz [2021]. In addition to these phase relationships, monazite shows a range of reaction textures that allow a finer interpretation of the ages obtained. Zoned metamorphic monazites are now currently documented [e.g., Soret et al., 2022]. Retrograde allanite ± apatite coronas around monazite can develop in metagranites and metapsammopelites. These can be dated *in situ* Hentschel et al. [2020] and provide a fine-scale constraint for retrograde paths. So-called "satellite" textures Finger et al. [2016], which are more difficult to date because finer, are also symptomatic of thermal events or retrograde fluid entry pulses.

The relationship between monazite and garnet is itself a topic of recurrent debate. Thermochemical considerations predict that monazite and garnet are not expected to grow together Spear and Pyle [2010], Kohn [2016]. In several cases, ages on monazites indeed frame ages on garnet [for instance, Godet et al., 2020b]. A study on cogenetic rock pairs showing or not garnet also highlights that monazites grow earlier in garnet-free rocks, and later in garnet-rich rocks Schulz and Krause [2018]. However, monazite grains as inclusions in garnet peritectic rims have been interpreted as the result of prograde breakdown of apatite under suprasolidus conditions Manzotti et al. [2018], Godet et al. [2021].

The extreme sensitivity of monazite to variations in the fluid regime of rocks makes them a hygro-petrochronological tool of choice Bosse and Villa [2019].

3.2. *Multi-method approach and the comparison of independent ages*

Multi-method petrochronological approach linking determination of PT path based on the rock chemistry, texturally-controlled dating of accessory and major phases, yields the best input for the thorough building of PTt-strain-fluids paths in mountain belts internal zones, but also feeds the debate about relative behaviors of the different chronometers with natural evidence.

In the Southeastern Churchill Province (SECP), Canada, quantitative P–T–t-strain-fluid paths were built by combining U–Pb zircon–monazite and Lu–Hf garnet dating with phase equilibrium modeling, empirical thermobarometry, and trace element mapping. Timing of initial collision, duration of anatexis, and pace of crustal assembly at mid-crustal levels were then estimated [Godet et al., 2021, Figure 6A]. A metatexite from the Tasiuyak Complex, yields a singular PTt evolution with garnet Lu–Hf date indistinguishable from U–Pb monazite age(Figure 6B), and older than U–Pb zircon age (Figure 6C). A core-to-rim decrease of Lu concentrations (Figure 6D) is consistent with preserved growth zoning and the authors interpreted the date as being weighted toward the timing of core crystallization in subsolidus conditions. Petrographic investigations show apatite inclusions within subsolidus garnet cores, and monazite in suprasolidus garnet rims and matrix (Figure 6E). Altogether, the Lu–Hf garnet chronometer constrains the timing of crustal thickening and sets a minimum age for the onset of continental collision; and the monazite and zircon U–Pb records bracket the duration of anatexis estimated at ~10 to 50 Myr [Figure 6F; Charette et al., 2021, Godet et al., 2021].

When compiling PTt paths based on multi-method approach in the case of UHP metamorphism, that encompasses the largest P and T variations McClelland and Lapen [2013] some general considerations arise: (i) the chronometer sequence depends at first order on the maximum temperature

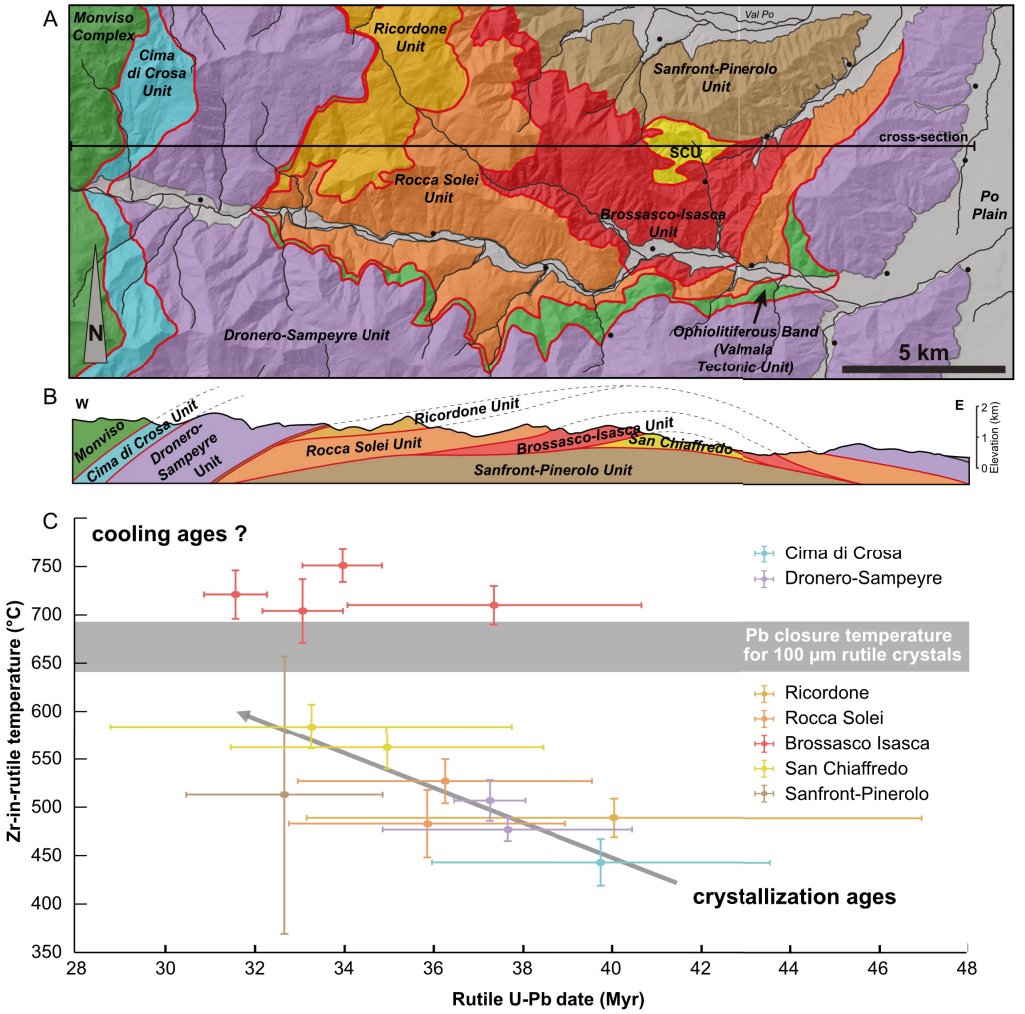

Figure 5. (A) Map of the Dora-Maira massif showing the existence of several subunits of subducted continental crust. (B) Cross-section showing the nappe-stack structure of the massif. (C) Combination of rutile U–Pb geochronology and Zr-in-rutile thermometry in high and ultrahigh-pressure rocks from the Dora-Maira massif, Western Alps [data from Bonnet et al., 2022]. Pb closure temperatures are evaluated at cooling rates between 10 and 100 °C/Myr, using diffusion parameters of Cherniak [2000]. Colors correspond to different units. Error bars are $\pm 2\sigma$.

reached. Along HP–LT gradients, rocks with PT paths remaining below 600 °C will tend to show prograde zircons, while rocks experiencing higher temperatures (above 700 °C) will tend to develop zircons along their retrograde path, controlled by interaction with melt Hermann et al. [2013], (ii) garnet grows along the prograde to peak temperature conditions in most cases. The distinct dating of cores and rims Tual et al. [2022], or the combined use of Lu–Hf and Sm–Nd Johnson et al. [2018], Charette et al. [2021] might even yield multiple ages along this interval and hence an estimate of tectonic processes rates (cf. Section 3.4) and (iii) monazite appears to be a trustful record of low-grade stages under subsolidus conditions, in most cases framing garnet growth [e.g. Godet et al., 2020b], even though equilibrium between the two phases has to be carefully assessed based on rock chemistry Hoisch et al. [2008], Kohn [2016]. Rutile has a more complex behavior and can be, in the same rock, shielded in garnet and then

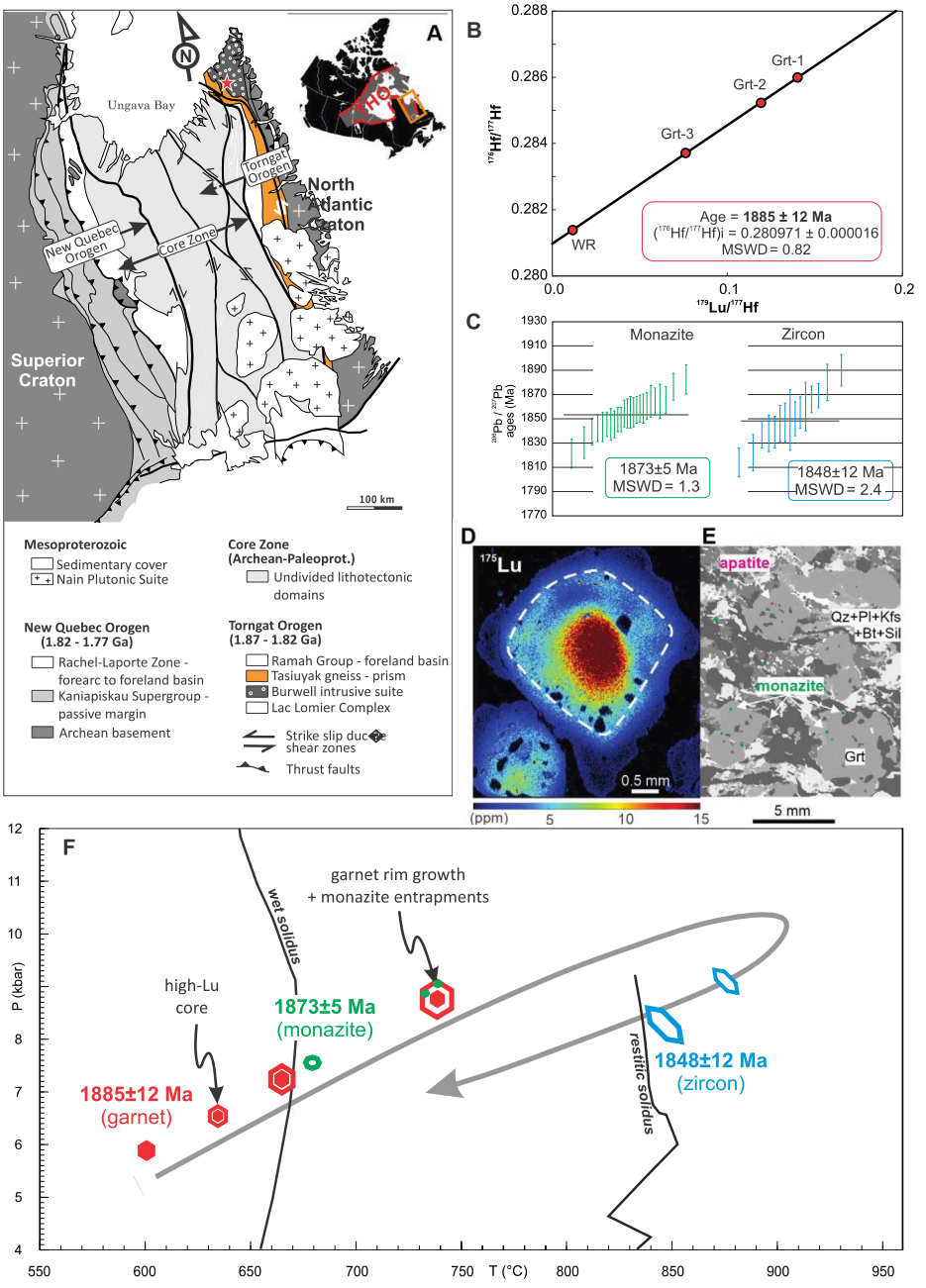

Figure 6. Composite figure modified after Godet et al. [2021]. (A) Simplified geological architecture of the Southeastern Churchill Province, Canada. The red star shows the location of the dated sample in northern Torngat Orogen. THO = Trans-Hudson Orogen. (B) Lu–Hf garnet isochron. WR = Whole rock; Grt = garnet fraction. (C) U–Pb monazite and zircon chronology. (D) Lutetium distribution in garnet (LA-ICP-MS map). (E) Grey-scaled microXRF image showing the textural location of accessory phases. We note that apatite (in pink) is exclusively observed in garnet-cores and monazite (in green) in garnet-rims and matrix. (F) Composite *P*–*T*–*t* path [modified after Godet et al., 2021]. The inferred *P*–*T* path is after Tettelaar and Indares [2007]. The wet and restitic solidii are from White et al. [2007] and Charette et al. [2021], respectively.

yields prograde ages or gives later ages when located in the matrix Bonnet et al. [2022], Jacob et al. [2022].

These rules of thumb however require to be discussed in the light of error propagation for ages stemming from different methods and labs. Indeed, ages obtained on different minerals, via different methods and in different labs need to be compared using the largest acceptation of uncertainty. Uncertainties stemming from the isotopic and elemental ratios uncertainty of the primary reference material must be added with uncertainty due to long-term excess variance of the secondary standard and the uncertainty on the used decay constant Horstwood et al. [2016]. For instance, for the multi-method PT-path produced for the Tasiuyak terrane, in the Churchill Province by Godet et al. [2021], the propagation of external errors on zircon ages does not significantly change the uncertainty on $^{207}Pb/^{206}Pb$ ages, which lays close to 10 Myr for 1900 Ma ages. Even though the used constant decay for lutetium is constrained by comparison with U–Pb ages Söderlund et al. [2004], the full uncertainty on Lu–Hf ages is close to twice the internal uncertainty, changing from 12 Myr to 20 Myr for 1900 Ma absolute values. In this regard, distinguishing tectono-metamorphic stages or evaluating rates over periods shorter than 30 Myr at 2000 Ma is actually impossible on the sole comparison of U–Pb zircon and Lu–Hf garnet ages.

3.3. *Campaign-style dating: spatial resolution in the field and statistical approach*

The methods based on laser ablation (LA-ICP-MS) and its sophistications now allow the massive production of *in situ* age data with textural and possibly geochemical control. This opens possibilities for mapping approaches at large geodynamic scale (e.g. orogen) as well as a statistical approach of the age distribution according to the methods used. Campaign-style *in situ* Lu–Hf analysis of garnets from 25 felsic gneisses, metapelites and migmatites from the Western Gneiss Region, Norway Tamblyn et al. [2022] resulted in the systematic distinction of unexpected inherited Neoproterozoic cores from Caledonian high-pressure overgrowth. Campaign-style *in situ* dating on titanites Mottram et al. [2019] over 2000 km of lateral continuity within the GHS reveals a continuous east–west gradient in titanite ages, correlated with an eastward decrease in GHS thickness. A lateral variation of the wedge dynamics (with later accreted and thicker units to the east) appears thanks to this study. So gaining spatial resolution at the thin-section scale comes together with gaining spatial resolution in the field.

Massive acquisition campaigns also produce such a quantity of homogeneous data in method and analytical error, that a statistical approach is possible, following the example of detrital zircon studies. Age frequency curves on different minerals (often zircon and monazite) can thus be used to decipher the different phases of a single metamorphic event in different units or to estimate the duration of this event [Taylor et al., 2016, Ding et al., 2021, Figure 7A,B]. Rather than assessing the peak timing, the frequently bimodal monazite and zircon age distribution curves allow to frame the regional temperature peak and estimate its duration. Such results actually constitute a breakthrough in the petrochronological data value as it assigns an age to the studied metamorphic events but also yields access to their duration and hence their characteristic time-scale.

3.4. *Assessing the duration of processes*

Thanks to the development of *in situ* analysis, modern geochronology techniques allow to date various texturally and chemically constrained mineral generations and estimate the duration of the processes associated with successive crystallization events. For example, dating the overall activation interval of shear zones is possible thanks to recrystallization caused by strain and the partial preservation of prior generations. This is the case in Syros, where the activity of the Lia shear zone was dated from 53 to 37 Ma using the ^{40}Ar–^{39}Ar *in situ* method Laurent et al. [2021].

Ages obtained in various minerals and/or generations can also be pinned along the PT path allowing to estimate the duration of burial and exhumation of metamorphic rocks. This is particularly the case with the multi-method approach, involving multiple geochronometers with various crystallization timing and/or diffusion resetting.

As an example, the residence duration of rocks in the supra-solidus domain in collision context is determined more and more precisely. As early as 2011, for example, titanite ages from the GHS calc-schists showed that the latter had resided in the

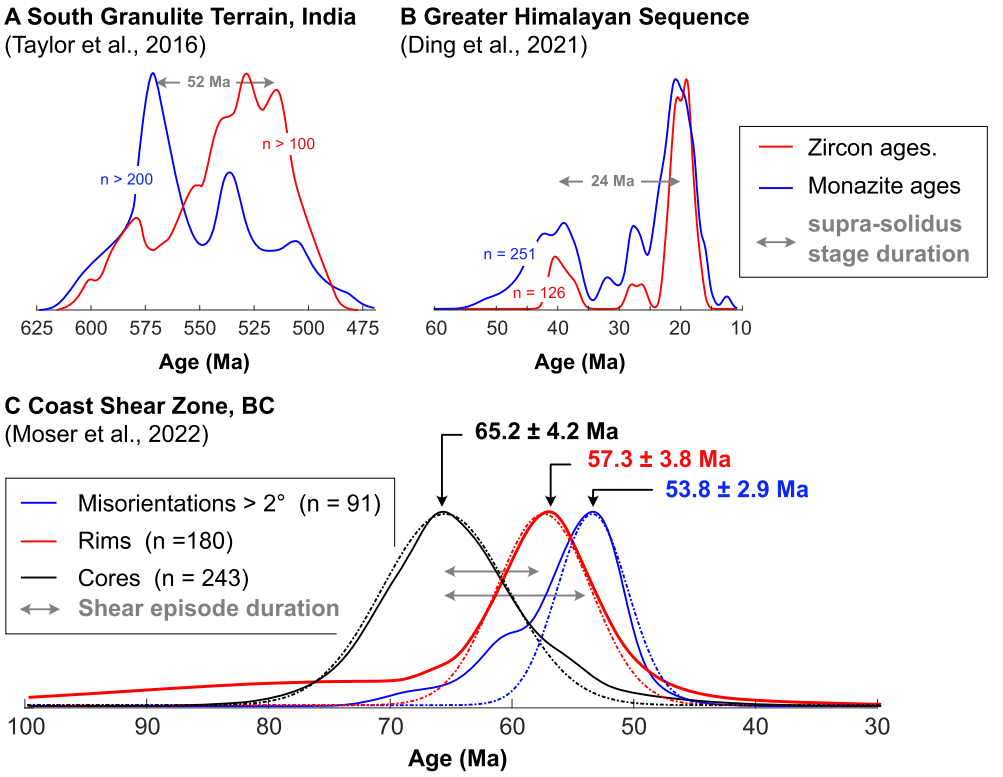

Figure 7. Comparison of zircon and monazite ages during process. Monazite and zircon U/Pb age distribution patterns for the South Granulite terrain, India (A) Taylor et al. [2016] and the Eastern Greater Himalayan Sequence in China (B) Ding et al. [2021] for partial melting duration. Histograms are built summing even normal distribution for each age. Duration of the partially molten stage is deduced from the time delay between retrograde zircon and prograde monazite age peaks. (C) Shear event in the Coast Shear Zone British Columbia, Canada Moser et al. [2022] from U–Pb age populations defined on the basis of intra-gran strain patterns deduced from EBSD analysis. Deformed grain domains are defined by an average misorientation of the analysis laser spot higher than 2°. Rims and cores are defined on the basis of Ce mapping. Dashed lines represent best Gaussian fits for main peak. Average ages given are centers and deviations for these.

supra-solidus domain for more than 10 Myr prior to the initiation of the Main Central Thrust Kohn and Corrie [2011]. Bimodal frequency curves of ages on monazite and zircon suggest that the duration of the supra-solidus phase could reach 22 to 24 Myr locally [Ding et al., 2021, Figure 7B]. In the Central Alps, zircon ages from migmatitic gneiss sampled along the Insubric Line Rubatto et al. [2009] also show a residence time of 10 Myr under anatexis conditions. The detailed age distribution implies that this 10 Myr period actually represents a succession of shorter time scale fluid ingression pulses responsible for partial melting Rubatto et al. [2009]. In older orogens [Eastern Ghats, India, Korhonen et al., 2013; Churchill Province, Canada, Charette et al., 2021, Godet et al., 2021] the molten state period can even reach 30 to 70 Myr respectively, according to the multi-method paths produced. The density and precision of the ages obtained today thus allow to highlight long partially molten stages within ancient or recent collisional systems. The evidence of these long-lasting stages implies that partial melting can last for a long time without inducing strain localization Kohn and Corrie [2011] and that partially molten systems probably constitute temperature-buffered reservoirs, capable of persisting under the joint

effects of latent heat of partial melting Labrousse et al. [2015], fluid circulations Rubatto et al. [2009], or shear heating Ding et al. [2021].

3.5. *Microstructural geochronology: using strain to interpret dates*

The usual approach to date a deformation event in high-grade rocks is to first establish a pressure–temperature–deformation path by identifying the paragenesis and their relationship to strain, then add absolute ages from accessory minerals by relative chronology to major phases (cf. Section 2.1.1), and thus obtain a pressure–temperature–time–deformation path. However, datable minerals can also be direct carriers of deformation markers. The joint use of *in situ* dating methods and grain-scale deformation analysis (e.g. EBSD, TEM or APT) allows to directly establish a link between isotopic signal and deformation.

In medium-temperature mylonites (amphibolite facies) from the Seve nappe, Norwegian Caledonides, EBSD analysis of titanite aggregates elongated in the mylonitic foliation Giuntoli et al. [2020] shows weak texturing, which is symptomatic of low internal plastic deformation and thus of efficient recrystallization during the formation of these aggregates. The U–Pb analysis on these aggregates, although discordant, gives well-constrained lower intercepts interpreted as the age of mylonitic foliation development. EBSD analysis of datable phases can on the other hand show strong textures symptomatic of active plastic deformation mechanisms in inherited minerals. In one zircon from a Siberian xenolith Timms et al. [2011], subgrain boundaries, defined by weak misorientations in EBSD maps, consistently show Ti depletion and REE enrichment relative to subgrain cores. These crystal-scale strain localization zones are also systematically poorer in Pb and thus appear younger than the host zircon, based on SHRIMP analyses. This precursor study shows that deformation-assisted REE and Pb redistribution processes are faster (by 5 orders of magnitude according to the authors) than temperature-activated diffusion.

In mylonitic gneiss calcsilicates from the Coast Shear Zone, British Columbia, the identification of bent zones characterized by strong disorientations and fluid-associated recrystallization rings has been coupled with *in situ* LASS analyses, which simultaneously provide ages, Zr contents, and REE spectra of ablated domains Moser et al. [2022]. A direct correlation appears between ages and misorientation, and the bent domains are statistically younger than the titanite rims and cores (Figure 7C). The question of interpreting this age difference as the duration of shear zone activation or as the effect of a single deformation event 10 Myr later than the initial crystallization of the titanites remains open Klepeis et al. [1998], Moser et al. [2022], but access to the duration of the deformation stage is within reach here.

The ultimate refinement in terms of correlation between isotopic signal and intra-crystalline structure comes from the application of atom probe tomography (APT) to silicates which opens the way to "nano-geochronology" Moser et al. [2017]. Mapping the exact position of each lead atom in the prepared sample allows the identification of heterogeneities in their distribution at the nanoscale. Tests have been carried out on ancient and therefore lead-rich accessory minerals for half a dozen years and open new perspectives. Coupled TEM and APT study of a monazite from Rogaland, Norway, shows that radiogenic Pb is concentrated in clusters that behave as closed nano-systems while the whole grain can be considered as an open system Seydoux-Guillaume et al. [2019]. The development of such nano-scale Pb clusters has been linked to the mineral strain in some cases. On 1.7 Ga monazites [Sandmata Complex, India, Fougerouse et al., 2021] from rocks deformed at 980 Ma, a coupled EBSD, TEM and APT approach shows that mechanically twinned domains are depleted in Pb. The nano-scale age calculated on the twinned domain corresponds to the age acknowledged for the deformation from coupled HR-EBSD and SHRIMP analysis Erickson et al. [2015]. It seems that lead is released during the shearing associated with the twinning by breaking and rearranging of the bonds with the oxygen ion framework which preferentially affects the Pb retention sites. The high dislocation density of the progressing twin tip could expel large Pb ions from the mineral at much higher rates than other recrystallization mechanisms.

It is therefore the deformation itself that is datable, in the cases where it acts as a much more efficient mechanism for resetting the isotopic signal than competing processes.

4. Discussion: impact of petrochronology data on deep tectonics concepts

The description of strain patterns in the inner zones of mountain belts is based on the definition of distinct tectonic units as finite volumes of rock, derived from the lower or upper colliding plate, with a defined paleogeographic origin and bounded by zones of localized strain. Understanding this finite deformation as the result of a continuous process or as a sequence of deformation phases (D_i) is a duality inherent to tectonic analysis Fossen et al. [2019]. Nevertheless, the distinction of successive metamorphic parageneses (M_i) and the collection of point ages associated directly or indirectly with these parageneses tend to provide a discrete or sequential picture of the time dimension of the evolution of the internal zones: each unit is characterized by a succession of deformation phases D_i and metamorphic imprints M_i, which distinguishes it from its surrounding counterparts. The increase in the spatial density of age data within and across these units, plus the increased precision of these ages, including for old processes (older than 1 Ga), and their association with one or several precise stages along PT paths, leads to (i) question the very notion of unit, (ii) question the meaning of the successions of different ages within the same unit, (iii) search for the spatial scale and thus the process that controls the age pattern and (iv) apprehend the possible secular variation of orogenic processes time scale.

4.1. *Questioning the notion of unit*

Campaign-style studies and regional compilations make it possible to map age patterns within domains of variable size [unit size: Cycladic Blueschists, Glodny and Ring, 2022, or the GHS, Mottram et al., 2019, massif scale: Lepontine Alps, Boston et al., 2017, internal zone: Western Gneiss Region, Wiest et al., 2021, or whole orogen: Capricorn orogen, Olierook et al., 2019]. In some cases, age distributions, in addition to the structural dataset, allow subunits to be distinguished.

In the Dora Maira nappe stack, HP to UHP subunits are distinguished thanks to metamorphic P–T gaps (up to 2 GPa and 250 °C) and diverse lithological compositions [e.g. Chopin et al., 1991, Groppo et al., 2019, Manzotti et al., 2022]. U–Pb ages obtained in rutile in the southern part of the massif, show a downward-decrease trend across the nappe-stack [Bonnet et al., 2022, Figure 5]. This is again consistent with the progressive burial of upper to lower units from ca. 40 to ca. 33 Ma. However, given the large maximum pressure (hence depth ?) differences between the units, the preservation of the paleogeographic order of units within the nappe stack implies that exhumation of each unit was so fast that the next unit only reaches peak after exhumation of the previous unit at least to similar depths. Fast exhumation rates for these units are in line with those calculated for the UHP unit of the massif by Rubatto and Hermann [2001]. The younger limit for exhumation of all units is a common retrogression event throughout the massif dated by U–Pb geochronology on titanite at ca. 33–32 Ma Rubatto and Hermann [2001], Bonnet et al. [2022]. Units significance is both paleogeographic and tectonic, and hence age and structural patterns coincide.

The paradigmatic section of the Upper Cycladic Blueschists Unit (UCBU, Figure 8) divided into 2 Schumacher et al. [2008], Glodny and Ring [2022] or 3 subunits Laurent et al. [2017, 2021], Kotowski et al. [2022] on the island of Syros, shows the relationships between PT evolution, age pattern and deformation at different scales. A consensus emerges that the UCBU evolved in a thermo-kinetically stationary subduction channel system Uunk et al. [2022], even though significant differences in exhumation PT path between some units are documented Trotet et al. [2001], Laurent et al. [2018]. The younging downward of HP stage ages evidences the progressive burial of upper to lower subunits from 51 to 43 Ma, as distal to proximal parts of a former passive margin Wijbrans et al. [1990], Glodny and Ring [2022], Kotowski et al. [2022], Uunk et al. [2022]. The evolution of Rb–Sr and ^{40}Ar–^{39}Ar ages on micas across these subunits is consistent with an increasing footprint of greenschist retrogression towards the bottom of the stack Laurent et al. [2021], Glodny and Ring [2022]. The age difference between HP stage and greenschist deformation yields a characteristic 10 Myr time interval for exhumation of these units Glodny and Ring [2022]. The debated delineation of subunits within the UCBU is based on lithological correlations, structural analysis, metamorphic grades, isotopic signal but also protolith and metamorphic ages (Figure 8). Increasing the density of protolithic and metamorphic ages allows to refine these subunits.

The distinction of the middle and lower allochthons based on strain analysis [Laurent et al., 2021, Figure 8A] produces monomodal ages patterns, while Kotowski et al. [2022] delineation yields a bimodal age pattern for the lower CBU. The uppermost/middle UCBU boundary is both a large-scale shear zone and an age shift in HP and retrogression stages Glodny and Ring [2022]. A systematic decrease in ^{40}Ar–^{39}Ar ages on phengites towards the core of the shear zones delineating these subunits is also observed at the decameter to hectometer scale Laurent et al. [2021]. The debated distinction between a lowermost and a middle unit, is actually supported by a local 15 Myr age gap across the Delfini shear zone Laurent et al. [2021], so that definition of tectonic units based on their age pattern cannot be elaborated on without a consideration of the sampling scale behind age populations.

In other cases, unit boundaries defined on protolith affinities and deformation localization do not match the contrasts inferred from age patterns. This is the case within the WGR, where the Blåhø nappe, defined as an equivalent of the Seve nappe allochthon Robinson [1995] reached UHP conditions during the Scandian collision. The mismatch in age patterns between the northern and southern portions implies that this allochthonous unit was disrupted into several subunits prior to its involvement in continental subduction, or that the different domains constitute two distinct units mixed up until now March et al. [2022]. The age distribution, especially prograde, within the WGR parautochthon also shows jumps that do not correspond to deformation localization zones. The eastward continuation of the major Nordfjord Shear Zone Labrousse et al. [2004] into the Lom Shear Zone Wiest et al. [2021] or even the Geiranger Shear Zone Young [2018] are supported more by jumps in age patterns than by structural evidence [Wiest et al., 2021, and Supplementary material]. Thus, it appears that in the deep dynamics of the convergence zones, age patterns and deformation patterns do not match as well as in more superficial systems. Extending the duplex accretionary prism model to converging systems involving metamorphism up to 500 °C and 1 GPa Angiboust et al. [2022] or more broadly the accretionary tectonics of small cold orogens [as opposed to large hot orogens, Chardon et al., 2009, Jamieson and Beaumont, 2013] indeed tends to show that considering tectono-metamorphic units as finite and coherent volumes over their entire PTt history is conclusive. The generalization of this approach to larger-scale structures, involving in particular high-temperature basement units possibly affected by anatexis, comes up against the complexity of age patterns. It would therefore be more relevant to consider that materials beyond a certain localized–distributed strain transition [deeper than the acknowledged brittle–ductile transition; Cooper et al., 2017] behave as continuous fluids in which the strain localization itself shows a timescale Girault et al. [2022] of the same order of magnitude as that of the movement of the materials (i.e. 10 Myr).

4.2. *The tectonic meaning of age sequences*

Multi-method studies in particular led to move petrochronology out of the M_i/D_i approach Oriolo et al. [2022] and to extend the progressive approach to the interpretation of age patterns. The documentation of several age populations in the same rock or unit, favored by the large number of dates produced and their interpretation as ages on the basis of textures or geochemical signatures, yields different conclusions depending on the time scale on which these populations are distributed. In the early Earth times, for example for the Warrawoona greenstone belt and the associated Mount Edgar granitoids in the Pilbara craton in Australia, two distinct metamorphic ages have been documented and assigned to distinct burial and exhumation cycles during sagduction processes, which are partial (and crustal) convective overturns between supracrustal greenstones/sediments cover and their granitoid basement at 3312 ± 5 Ma (U–Pb on zircon) and 3343 ± 5 Ma [U–Pb on monazite inclusions trapped in garnet; François et al., 2014]. Interestingly, the recorded PTt conditions support fast, gravity-driven tectonics, where surface sedimentary rocks were buried until lower crust conditions and exhumed back to the surface in less than 10 Myr. Over a shorter interval, in the Seve nappe complex (SNC) of the Norwegian Caledonides, Walczak et al. [2022] distinguished two successive burial stages at 483 ± 4 Ma and 439 ± 4 Ma by laser ablation depth-profiling on zircons. The distinction of two types of age profiles and geochemical signatures allowed the old age to be associated with eclogite facies and the young one with granulite

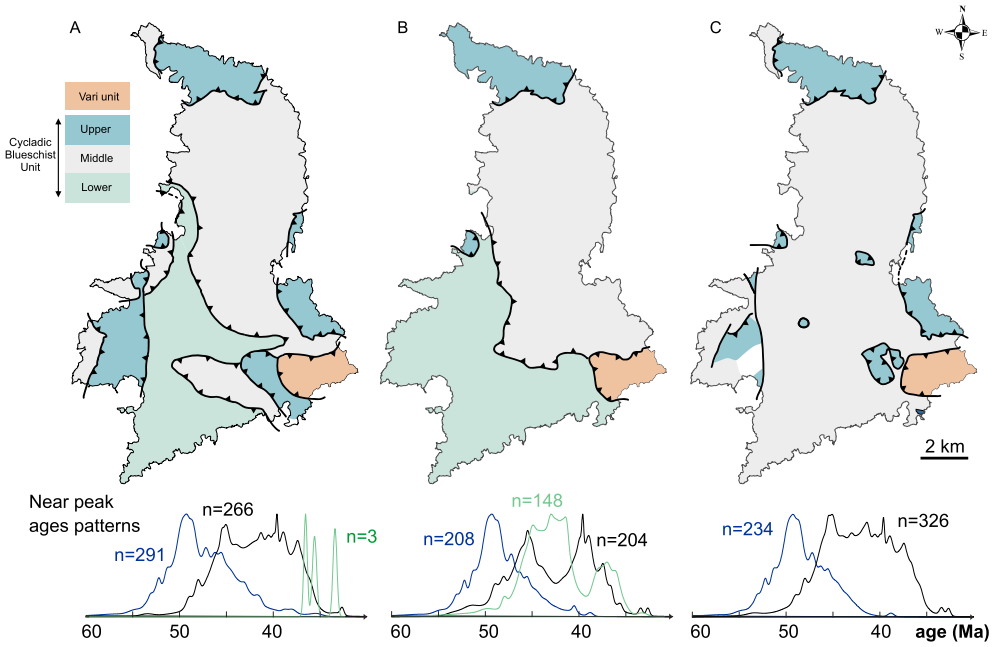

Figure 8. Comparison of the proposed subunits delineation in Syros from (A) Laurent et al. [2016], (B) Kotowski et al. [2022] and (C) Glodny and Ring [2022] associated with the literature near-peak ages depending on this delineation. For age compilation see Glodny and Ring [2022] and Gyomlai et al. [2023].

facies, consistent with two successive decompression episodes after a first peak of HP and a second of HT. These are therefore not just points that are dated along the PT path but trends. The new HP stage in the SNC, 20 Myr older than regionally documented [460 Ma, Brueckner and Van Roermund, 2007] is interpreted as the signature of successive burials of the same unit in the same convergence zone. A similar petrochronological approach on zircon, titanite and allanite from gneiss of the Sesia zone, Italian Alps Rubatto et al. [2011], is also consistent with two successive burial stages in the eclogite facies, less than 20 Myr apart.

Such PTt paths support the "Yo-yo subduction" model, first proposed on the basis of thermochronology and sedimentology data in the Nigde Massif, Turkey Umhoefer et al. [2007] on a time scale of about 60 Myr. In the case of the Nigde Massif, the recurrence of HP stages is attributed to changes in boundary conditions along a strike-slip shear zone [the Central Anatolian Fault Zone, Umhoefer et al., 2007]. Other interpretations of Yo-yo subduction do not rely on changes in boundary conditions to explain successive tectonic–metamorphic events but on material displacement in a stationary subduction system. The estimated time intervals (20 ± 10 Myr) would then be a characteristic time for the circulation of matter in the subduction interface Agard et al. [2009] unless it is the finest grain at which we can distinguish different events. Stages have actually been distinguished over shorter intervals, like for instance the four successive phases of growth recorded over 20 Myr by zircon from the high-deformation metasedimentary mélange of the Nirgua Complex, in the Venezuelan Cordillera Viete et al. [2015]. The method used reproduces with comparable resolution the results of previous thermochronology studies, and modifies their previous interpretation as a thermal signal. The different episodes are supposed to last less than 1 Myr with a recurrence time of 5 Myr and represent either thermal pulses or pulses of fluid arrival during a single metamorphic event. In Western Papua New Guinea, U–Pb ages obtained on zircon from HP metasedimentary rocks and eclogites highlight a very fast burial and exhumation in less than 10 Myr François et al. [2016]. Similarly,

Eastern Papua records an UHP metamorphic event (with coesite occurrence) at ca. 4 Ma Baldwin et al. [2004]. These two examples are the youngest documented eclogites exposed in the Earth surface. The significance of these very short time scales can be understood either as short-term variations in boundary conditions (heat advection, fluid flow) for a volume of rock that is moving on a longer time scale or as the rapid movement of the volume of rock in boundary conditions that are evolving on a longer time scale (in the case of a long-lived as in Papua-New Guinea). In both cases it is the competition between advective processes (of fluids or solids) and diffusion processes (of heat or fluids) that controls the actual time scale documented. Fully coupled thermo-mechanical numerical models of subduction systems produce complex PTt paths during the progressive individualization of oceanic units in subduction settings with notably transient decompression on the order of 0.5 GPa on time scales of 2 to 3 Myr Blanco-Quintero et al. [2011], Ruh et al. [2015]. The state-of-the-art resolution of petrochronology thus provides a tectonic meaning to the complex path shapes predicted by thermo-mechanical models [Gerya, 2022, and references therein].

4.3. *Secular evolution of geodynamic processes*

The accumulation of ages obtained on HP–LT metamorphic rocks [with pressures higher than 2.5 GPa and or thermal gradients lower than 300 K/GPa, Brown and Johnson, 2018] yielded the identification of their massive emergence to the Neoproterozoic (at the end of the Tonian i.e. 700 Ma) which has been interpreted as the signature of the appearance of modern plate tectonics on Earth Stern [2005]. This data is undoubtedly altered by preservation bias, due on the one hand to retrogression and polymetamorphism, as complex as the rocks are old Palin et al. [2020], but also due to the erosion of the superficial parts of ancient orogenic wedges in which HP–LT relics are most often imbricated Willigers et al. [2002]. The continual addition of older ages to the list of HP–LT metamorphic occurrences Palin et al. [2020], Brown et al. [2022] is likely evidence of such a preservation bias.

This being said, the occurrence of HP–LT minerals or parageneses is not unequivocal evidence for the establishment of modern tectonics. First, local production of HP rock does not imply the establishment of global plate tectonics Dewey et al. [2021]. Indeed, crustal-scale sagduction tectonics is prone to produce metamorphic rocks with PTt paths undistinguishable from modern tectonics [0.9–1.1 GPa and 450–550 °C i.e. 500 K/GPa; François et al., 2014]. The only difference is actually the space scale of the metamorphic pattern: lithospheric for modern-day subduction vs crustal for sagduction and the maximum of pressure reached.

(Ultra) High Pressure–Low Temperature ((U)HP–LT) metamorphic rocks such as eclogites provide crucial clues for the geodynamic processes, as these rocks have only been described in modern orogens. Indeed, the PTt conditions recorded by the eclogites and some index minerals they contain (e.g. omphacite, coesite, glaucophane, lawsonite, carpholite) are indisputable indicators of the presence of a deep subduction involving the burial of a relatively cold crust in the mantle at great depth (>70 km). These types of rocks are not produced in the Archean Agard et al. [2005], Brown and Johnson [2018] where the maximum recorded pressures do not exceed 1.5 GPa (Figure 9). A transition period during the Paleoproterozoic records the first occurrences of eclogites worldwide during the amalgamation of the Columbia/Nuna Supercontinent François et al. [2018, 2022], even if no UHP markers (such as coesite) are observable (Figure 9). HP metamorphic rocks could also betray strong stress deviators, and thus significant mean pressures without significant burial in convergence zones Yamato and Brun [2017]. It is beyond the scope of this paper to discuss the significance of the pressures recorded by metamorphic rocks Hobbs and Ord [2017], but in any case, the occurrence of (U)HP–LT (>1.5 GPa) metamorphic rocks over large spatial scales does reflect the development of a strong lithosphere prone to subducting or supporting high stress deviators.

Multi-method approach further allows to estimate time intervals for one same rock or unit and thus to access rates, so far underutilized in the debate on the secular evolution of Earth dynamics Chowdhury et al. [2021]. Provided that age differences are compared accounting their complete source of uncertainties, differences between the age of metasedimentary detrital rock protoliths, inferred from detrital zircons for ancient times, and the age of metamorphism allow to assess, along with an estimate of the maximum

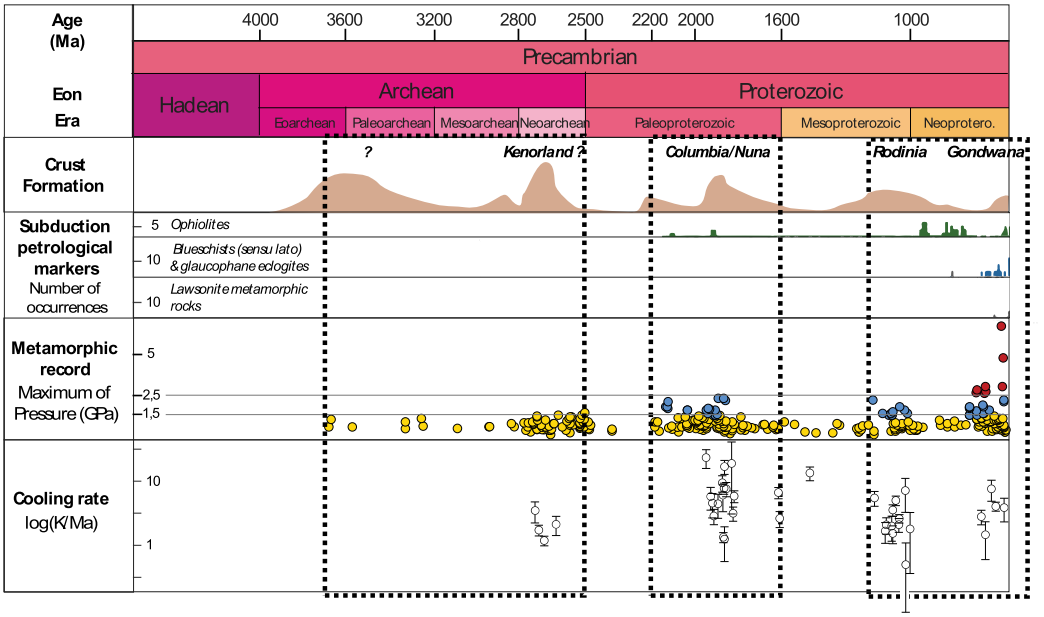

Figure 9. Evolution of metamorphism markers through Precambrian times [data from Stern and Gerya, personal communication and Brown and Johnson, 2018]. Yellow circles: $P < 1.5$ GPa, blue circles: P 1.5 to 2.5 GPa, red circles: $P > 2.5$ GPa. Cooling rates deduced from metamorphic rocks PTt paths over the 4 Ga geological record [data Brown et al., 2022]. Conservative estimates of uncertainties of ±50 °C on temperatures and ±5% on ages have been extended to cooling rates values.

depth reached, an apparent burial rate (in km/Myr) characteristic of the incorporation of foreland basins into their related wedge. The compilation of available estimates Nicoli et al. [2016] shows a secular decrease in the calculated maximum rates attributed to the gradual decrease in juvenile crust production as well as a decrease in the diversity of active orogenic processes Nicoli et al. [2016], Palin et al. [2020]. The age difference between metamorphic peak and retrogression assemblages allows, together with the estimate of associated T conditions, to calculate cooling rates [in °C/Myr, Chowdhury et al., 2021, Brown et al., 2022, Figure 9]. Solid diffusion profile modeling, or geospeedometry, yields comparable trends but the systematic one order-of-magnitude discrepancy between the two methods likely suggests that different things are being measured Viete and Lister [2017], Brown et al. [2022]. The secular trend in both cases is an exponential increase in cooling rate with time, with perhaps a jump in the early Phanerozoic, revealed by fine statistical analysis of the limited data set Brown et al. [2022] over the complete Earth history, although the restriction of the same data set to Precambrian times only does not show any trend (Figure 9). The cooling rates are also anti-correlated with the T/P gradients [Brown et al., 2022, Supplementary material]. These trends support the model of a gradual shift in orogenic dynamics from large hot peel-back orogens Chowdhury et al. [2017] where large heat flows limit the capacity of lithospheric rocks to localize strain Chardon et al. [2009], Gapais et al. [2009] to smaller and colder orogens where early and perennial localization of deformation allows for large relative vertical motions of the tectonic units, and thus larger cooling rates. Although the effect of external dynamics on the secular evolution of tectonics is not negligible, including the lubrication and stabilization of subduction zones by sedimentary inputs to the trench Sobolev and Brown [2019], it appears that the characteristic depth of the distributed–localized strain transition Cooper et al. [2017] that separates shallow and deep orogen dynamics Labrousse et al. [2004] or suprastructure and infrastructure Culshaw et al. [2006] appears to be the first-order parameter that controls the characteristic operating time of orogenic systems.

5. Conclusion

While the understanding of inner mountain belts evolved from the mapping of their structural and metamorphic boundaries in the field, to the understanding of thermo–chemo–mechanical processes behind the strain, fluid flow and reactions localization in space and time, petrochronology emerged, based on the interpretation of *in situ* ages in the light of geochemical and microstructural data acquired at the scale of tenth of microns analysis spots. The wealth of data produced now allows to estimate the duration of crucial processes along PTt path, such as the residence time in the supra-solidus domain, or the characteristic time of strain localization within the crust. Even if propagation of errors still blurs the image we have of the early Earth geodynamics, the precision, accuracy and amount of data produced by dating techniques allows campaign-style exploration of large portions of inner mountain belts, and lead to a more dynamic definition of tectonometamorphic units. Age patterns within or across these units emphasize that they only behave as finite and coherent bodies in the shallowest structural levels of orogenic wedges, and behave more as continuous visco-plastic fluids at greater depth and temperature, in which strain localization itself has a characteristic time, and inheritance-related mechanical contrasts only play a minor role.

The next step forward shall come from the coupling of *in situ* dating techniques with strain analysis at the same (EBSD) or higher (APT) resolution. These approaches should shortcut the long path that we still have to walk to pin strain and ages along a same pressure–temperature path, as it directly evidences the links between isotopes retention or diffusion and crystal lattice defaults.

Declaration of interests

The authors do not work for, advise, own shares in, or receive funds from any organization that could benefit from this article, and have declared no affiliations other than their research organizations.

References

Agard, P., Omrani, J., Jolivet, L., and Mouthereau, F. (2005). Convergence history across Zagros (Iran): constraints from collisional and earlier deformation. *Int. J. Earth Sci.*, 94, 401–419.

Agard, P., Yamato, P., Jolivet, L., and Burov, E. (2009). Exhumation of oceanic blueschists and eclogites in subduction zones: timing and mechanisms. *Earth Sci. Rev.*, 92(1–2), 53–79.

Airaghi, L., Warren, C. J., de Sigoyer, J., Lanari, P., and Magnin, V. (2018). Influence of dissolution/reprecipitation reactions on metamorphic greenschist to amphibolite facies mica $^{40}Ar/^{39}Ar$ ages in the Longmen Shan (eastern Tibet). *J. Metamorph. Geol.*, 36(7), 933–958.

Angiboust, S., Menant, A., Gerya, T., and Oncken, O. (2022). The rise and demise of deep accretionary wedges: A long-term field and numerical modeling perspective. *Geosphere*, 18(1), 69–103.

Armstrong, R. L., Jäger, E., and Eberhardt, P. (1966). A comparison of K–Ar and Rb–Sr ages on Alpine biotites. *Earth Planet. Sci. Lett.*, 1(1), 13–19.

Arnold, A. and Jäger, E. (1965). Rb–Sr Altersbestimmungen an Glimmern im Grenzbereich zwischen voralpinen Alterswerten und alpiner Verjüngung der Biotite. *Eclogae Geol. Helv.*, 58, 369–390.

Baldwin, S. L., Monteleone, B. D., Webb, L. E., Fitzgerald, P. G., Grove, M., and June Hill, E. (2004). Pliocene eclogite exhumation at plate tectonic rates in eastern Papua New Guinea. *Nature*, 431(7006), 263–267.

Barrell, J. (1914). The strength of the Earth's crust. *J. Geol.*, 22(7), 655–683.

Barrell, J. (1917). Rhythms and the measurement of geologic time. *Bull. Geol. Soc. Am.*, 28, 745–904.

Baxter, E. F., Caddick, M. J., and Dragovic, B. (2017). Garnet: A rock-forming mineral petrochronometer. *Rev. Mineral. Geochem.*, 83(1), 469–533.

Blanco-Quintero, I. F., García-Casco, A., and Gerya, T. V. (2011). Tectonic blocks in serpentinite mélange (eastern Cuba) reveal large-scale convective flow of the subduction channel. *Geology*, 39(1), 79–82.

Bloch, E. and Ganguly, J. (2015). 176 Lu–176 Hf geochronology of garnet II: numerical simulations of the development of garnet–whole-rock 176 Lu–176 Hf isochrons and a new method for constraining the thermal history of metamorphic rocks. *Contrib. Mineral. Petrol.*, 169, 1–16.

Bonnet, G., Chopin, C., Locatelli, M., Kylander-Clark, A. R., and Hacker, B. R. (2022). Protracted subduction of the European hyperextended margin re-

vealed by rutile U–Pb geochronology across the Dora-Maira massif (Western Alps). *Tectonics*, 41(4), article no. e2021TC007170.

Bosse, V. and Villa, I. M. (2019). Petrochronology and hygrochronology of tectono-metamorphic events. *Gondwana Res.*, 71, 76–90.

Boston, K. R., Rubatto, D., Hermann, J., Engi, M., and Amelin, Y. (2017). Geochronology of accessory allanite and monazite in the Barrovian metamorphic sequence of the Central Alps, Switzerland. *Lithos*, 286, 502–518.

Brown, M. and Johnson, T. (2018). Secular change in metamorphism and the onset of global plate tectonics. *Am. Mineral.*, 103(2), 181–196.

Brown, M., Johnson, T., and Spencer, C. J. (2022). Secular changes in metamorphism and metamorphic cooling rates track the evolving plate-tectonic regime on Earth. *J. Geol. Soc.*, 179(5), article no. jgs2022-050.

Brueckner, H. K. and Van Roermund, H. L. (2007). Concurrent HP metamorphism on both margins of Iapetus: Ordovician ages for eclogites and garnet pyroxenites from the Seve Nappe Complex, Swedish Caledonides. *J. Geol. Soc.*, 164(1), 117–128.

Chardon, D., Gapais, D., and Cagnard, F. (2009). Flow of ultra-hot orogens: a view from the Precambrian, clues for the Phanerozoic. *Tectonophysics*, 477(3–4), 105–118.

Charette, B., Godet, A., Guilmette, C., Davis, D. W., Vervoort, J., Kendall, B., et al. (2021). Long-lived anatexis in the exhumed middle crust of the Torngat Orogen: Constraints from phase equilibria modeling and garnet, zircon, and monazite geochronology. *Lithos*, 388, article no. 106022.

Cherniak, D. J. (2000). Pb diffusion in rutile. *Contrib. Mineral. Petrol.*, 139(2), 198–207.

Chopin, C., Henry, C., and Michard, A. (1991). Geology and petrology of the coesite-bearing terrain, Dora Maira massif, Western Alps. *Eur. J. Mineral.*, 3(2), 263–291.

Chowdhury, P., Chakraborty, S., and Gerya, T. V. (2021). Time will tell: secular change in metamorphic timescales and the tectonic implications. *Gondwana Res.*, 93, 291–310.

Chowdhury, P., Gerya, T., and Chakraborty, S. (2017). Emergence of silicic continents as the lower crust peels off on a hot plate-tectonic Earth. *Nat. Geosci.*, 10(9), 698–703.

Cochrane, R., Spikings, R. A., Chew, D., Wotzlaw, J. F., Chiaradia, M., Tyrrell, S., et al. (2014). High temperature (>350 °C) thermochronology and mechanisms of Pb loss in apatite. *Geochim. Cosmochim. Acta*, 127, 39–56.

Cooper, F. J., Platt, J. P., and Behr, W. M. (2017). Rheological transitions in the middle crust: insights from Cordilleran metamorphic core complexes. *Solid Earth*, 8(1), 199–215.

Culshaw, N. G., Beaumont, C., and Jamieson, R. A. (2006). The orogenic superstructure-infrastructure concept: Revisited, quantified, and revived. *Geology*, 34(9), 733–736.

Cutts, J. A., Smit, M. A., Kooijman, E., and Schmitt, M. (2019). Two-stage cooling and exhumation of deeply subducted continents. *Tectonics*, 38(3), 863–877.

Davis, D. W., Krogh, T. E., and Williams, I. S. (2003). Historical development of zircon geochronology. *Rev. Mineral. Geochem.*, 53(1), 145–181.

Dewey, J. F., Kiseeva, E. S., Pearce, J. A., and Robb, L. J. (2021). Precambrian tectonic evolution of earth: an outline. *South Afr. J. Geol.*, 124(1), 141–162.

Didier, A., Bosse, V., Bouloton, J., Mostefaoui, S., Viala, M., Paquette, J. L., et al. (2015). NanoSIMS mapping and LA-ICP-MS chemical and U–Th–Pb data in monazite from a xenolith enclosed in andesite (Central Slovakia Volcanic Field). *Contrib. Mineral. Petrol.*, 170, 1–21.

Ding, H., Kohn, M. J., and Zhang, Z. (2021). Long-lived (ca. 22–24 Myr) partial melts in the eastern Himalaya: Petrochronologic constraints and tectonic implications. *Earth Planet. Sci. Lett.*, 558, article no. 116764.

Dodson, M. H. (1973). Closure temperature in cooling geochronological and petrological systems. *Contrib. Mineral. Petrol.*, 40(3), 259–274.

Engi, M., Lanari, P., and Kohn, M. J. (2017). Significant ages—An introduction to petrochronology. *Rev. Mineral. Geochem.*, 83(1), 1–12.

Erickson, T. M., Pearce, M. A., Taylor, R. J. M., Timms, N. E., Clark, C., Reddy, S. M., and Buick, I. S. (2015). Deformed monazite yields high-temperature tectonic ages. *Geology*, 43(5), 383–386.

Finger, F., Krenn, E., Schulz, B., Harlov, D., and Schiller, D. (2016). "Satellite monazites" in polymetamorphic basement rocks of the Alps: Their origin and petrological significance. *Am. Mineral.*, 101(5), 1094–1103.

Fossen, H., Cavalcante, G. C. G., Pinheiro, R. V. L., and

Archanjo, C. J. (2019). Deformation–progressive or multiphase? *J. Struct. Geol.*, 125, 82–99.

Foster, G., Gibson, H. D., Parrish, R., Horstwood, M., Fraser, J., and Tindle, A. (2002). Textural, chemical and isotopic insights into the nature and behaviour of metamorphic monazite. *Chem. Geol.*, 191(1–3), 183–207.

Fougerouse, D., Reddy, S. M., Seydoux-Guillaume, A. M., Kirkland, C. L., Erickson, T. M., Saxey, D. W., et al. (2021). Mechanical twinning of monazite expels radiogenic lead. *Geology*, 49(4), 417–421.

François, C., de Sigoyer, J., Pubellier, M., Bailly, V., Cocherie, A., and Ringenbach, J. C. (2016). Short-lived subduction and exhumation in Western Papua (Wandamen peninsula): co-existence of HP and HT metamorphic rocks in a young geodynamic setting. *Lithos*, 266, 44–63.

François, C., Debaille, V., Paquette, J. L., Baudet, D., and Javaux, E. J. (2018). The earliest evidence for modern-style plate tectonics recorded by HP–LT metamorphism in the Paleoproterozoic of the Democratic Republic of the Congo. *Sci. Rep.*, 8(1), article no. 15452.

François, C., Philippot, P., Rey, P., and Rubatto, D. (2014). Burial and exhumation during Archean sagduction in the East Pilbara granite-greenstone terrane. *Earth Planet. Sci. Lett.*, 396, 235–251.

François, C., Pubellier, M., Robert, C., Bulois, C., Jamaludin, S. N. F., Oberhänsli, R., et al. (2022). Temporal and spatial evolution of orogens: A guide for geological mapping. *Episodes J. Int. Geosci.*, 45(3), 265–283.

Gapais, D., Cagnard, F., Gueydan, F., Barbey, P., and Ballèvre, M. (2009). Mountain building and exhumation processes through time: inferences from nature and models. *Terra Nova*, 21(3), 188–194.

Gardés, E. and Montel, J. M. (2009). Opening and resetting temperatures in heating geochronological systems. *Contrib. Mineral. Petrol.*, 158(2), 185–195.

Gervais, F. and Crowley, J. L. (2017). Prograde and near-peak zircon growth in a migmatitic pelitic schist of the southeastern Canadian Cordillera. *Lithos*, 282, 65–81.

Gerya, T. (2022). Numerical modeling of subduction: State of the art and future directions. *Geosphere*, 18(2), 503–561.

Gilotti, J. A. (1993). Discovery of a medium-temperature eclogite province in the Caledonides of North-East Greenland. *Geology*, 21(6), 523–526.

Gilotti, J. A. and McClelland, W. C. (2007). Characteristics of, and a tectonic model for, ultrahigh-pressure metamorphism in the overriding plate of the Caledonian orogen. *Int. Geol. Rev.*, 49(9), 777–797.

Girault, J. B., Bellahsen, N., Bernet, M., Pik, R., Loget, N., Lasseur, E., et al. (2022). Exhumation of the Western Alpine collisional wedge: New thermochronological data. *Tectonophysics*, 822, article no. 229155.

Giuntoli, F., Menegon, L., Warren, C. J., Darling, J., and Anderson, M. W. (2020). Protracted shearing at midcrustal conditions during large-scale thrusting in the Scandinavian Caledonides. *Tectonics*, 39(9), article no. e2020TC006267.

Glodny, J. and Ring, U. (2022). The Cycladic Blueschist Unit of the Hellenic subduction orogen: Protracted high-pressure metamorphism, decompression and reimbrication of a diachronous nappe stack. *Earth Sci. Rev.*, 224, article no. 103883.

Godet, A., Guilmette, C., Labrousse, L., Davis, D. W., Smit, M. A., Cutts, J. A., et al. (2020a). Complete metamorphic cycle and long-lived anatexis in the c. 2.1 Ga Mistinibi Complex, Canada. *J. Metamorph. Geol.*, 38(3), 235–264.

Godet, A., Guilmette, C., Labrousse, L., Smit, M. A., Cutts, J. A., Davis, D. W., and Vanier, M. A. (2021). Lu–Hf garnet dating and the timing of collisions: Palaeoproterozoic accretionary tectonics revealed in the Southeastern Churchill Province, Trans-Hudson Orogen, Canada. *J. Metamorph. Geol.*, 39(8), 977–1007.

Godet, A., Guilmette, C., Labrousse, L., Smit, M. A., Davis, D. W., Raimondo, T., et al. (2020b). Contrasting PTt paths reveal a metamorphic discontinuity in the New Quebec Orogen: Insights into Paleoproterozoic orogenic processes. *Precambrian Res.*, 342, article no. 105675.

Groppo, C., Ferrando, S., Gilio, M., Botta, S., Nosenzo, F., Balestro, G., et al. (2019). What's in the sandwich? New P–T constraints for the (U) HP nappe stack of southern Dora-Maira Massif (Western Alps). *Eur. J. Mineral.*, 31(4), 665–683.

Gyomlai, T., Agard, P., Marschall, H. R., and Jolivet, L. (2023). Hygrochronometry of punctuated metasomatic events during exhumation of the Cycladic blueschist unit (Syros, Greece). *Terra Nova*, 35(2), 101–112.

Hayden, L. A., Watson, E. B., and Wark, D. A. (2008).

A thermobarometer for sphene (titanite). *Contrib. Mineral. Petrol.*, 155, 529–540.

Henrichs, I. A., Chew, D. M., O'Sullivan, G. J., Mark, C., McKenna, C., and Guyett, P. (2019). Trace element (Mn-Sr-Y-Th-REE) and U–Pb isotope systematics of metapelitic apatite during progressive greenschist-to amphibolite-facies Barrovian metamorphism. *Geochem. Geophys. Geosyst.*, 20(8), 4103–4129.

Hentschel, F., Janots, E., Trepmann, C. A., Magnin, V., and Lanari, P. (2020). Corona formation around monazite and xenotime during greenschist-facies metamorphism and deformation. *Eur. J. Mineral.*, 32(5), 521–544.

Hermann, J., Rubatto, D., Korsakov, A., and Shatsky, V. S. (2001). Multiple zircon growth during fast exhumation of diamondiferous, deeply subducted continental crust (Kokchetav Massif, Kazakhstan). *Contrib. Mineral. Petrol.*, 141, 66–82.

Hermann, J., Zheng, Y. F., and Rubatto, D. (2013). Deep fluids in subducted continental crust. *Elements*, 9(4), 281–287.

Hobbs, B. E. and Ord, A. (2017). Pressure and equilibrium in deforming rocks. *J. Metamorph. Geol.*, 35(9), 967–982.

Hogmalm, K. J., Zack, T., Karlsson, A. K. O., Sjöqvist, A. S., and Garbe-Schönberg, D. (2017). In situ Rb–Sr and K–Ca dating by LA-ICP-MS/MS: an evaluation of N_2O and SF_6 as reaction gases. *J. Anal. At. Spectrom.*, 32(2), 305–313.

Hoisch, T. D., Wells, M. L., and Grove, M. (2008). Age trends in garnet-hosted monazite inclusions from upper amphibolite facies schist in the northern Grouse Creek Mountains, Utah. *Geochim. Cosmochim. Acta*, 72(22), 5505–5520.

Holder, R. M., Hacker, B. R., Kylander-Clark, A. R., and Cottle, J. M. (2015). Monazite trace-element and isotopic signatures of (ultra) high-pressure metamorphism: Examples from the Western Gneiss Region, Norway. *Chem. Geol.*, 409, 99–111.

Holmes, A. (1911). The duration of geological time. *Nature*, 87(2175), 9–10.

Holmes, A. (1928). *Radioactivity and Continental Drift*. Stephen Austin & Sons Limited, Hertford.

Horstwood, M. S., Košler, J., Gehrels, G., Jackson, S. E., McLean, N. M., Paton, C., et al. (2016). Community-derived standards for LA-ICP-MS U-(Th-) Pb geochronology–Uncertainty propagation, age interpretation and data reporting. *Geostand. Geoanal. Res.*, 40(3), 311–332.

Ibañez-Mejia, M., Pullen, A., Pepper, M., Urbani, F., Ghoshal, G., and Ibañez-Mejia, J. C. (2018). Use and abuse of detrital zircon U–Pb geochronology—A case from the Río Orinoco delta, eastern Venezuela. *Geology*, 46(11), 1019–1022.

Jacob, J. B., Janots, E., Guillot, S., Rubatto, D., Fréville, K., Melleton, J., and Faure, M. (2022). HT overprint of HP granulites in the Oisans–Pelvoux massif: Implications for the dynamics of the Variscan collision in the external western Alps. *Lithos*, 416, article no. 106650.

Jäger, E. (1962). Rb–Sr age determinations on micas and total rocks from the Alps. *J. Geophys. Res.*, 67(13), 5293–5306.

Jäger, E. (1967). Die Bedeutung der Biotit-Alterswerte. In Jäger, E., Niggli, E., and Wenk, E., editors, *Rb–Sr Alterbestmmungen an Glimmern der Zentralalpen*, Beitr. Geol. Kaarte Schweiz, NF, 134, pages 28–31. Kümmerli & Frey, Bern.

Jäger, E., Geiss, J., Niggli, E., Streckeisen, A., Wenk, E., and Wüthrich, H. (1961). Rb–Sr-Alter an Gesteinsglimmern der Schweizer Alpen. *Schweiz. Mineral. Petrogr. Mitt.*, 41(2), 255–272.

Jamieson, R. A. and Beaumont, C. (2013). On the origin of orogens. *Bulletin*, 125(11–12), 1671–1702.

Janots, E., Engi, M., Berger, A., Allaz, J., Schwarz, J. O., and Spandler, C. (2008). Prograde metamorphic sequence of REE minerals in pelitic rocks of the Central Alps: implications for allanite–monazite–xenotime phase relations from 250 to 610 °C. *J. Metamorph. Geol.*, 26(5), 509–526.

Jegal, Y., Zimmermann, C., Reisberg, L., Yeghicheyan, D., Cloquet, C., Peiffert, C., et al. (2022). Characterisation of Reference Materials for In Situ Rb–Sr Dating by LA-ICP-MS/MS. *Geostand. Geoanal. Res.*, 46(4), 645–671.

Johnson, T. A., Vervoort, J. D., Ramsey, M. J., Aleinikoff, J. N., and Southworth, S. (2018). Constraints on the timing and duration of orogenic events by combined Lu–Hf and Sm–Nd geochronology: an example from the Grenville orogeny. *Earth Planet. Sci. Lett.*, 501, 152–164.

Kelsey, D. E., Clark, C., and Hand, M. (2008). Thermobarometric modelling of zircon and monazite growth in melt-bearing systems: Examples using model metapelitic and metapsammitic granulites. *J. Metamorph. Geol.*, 26(2), 199–212.

Kirkland, C. L., Yakymchuk, C., Szilas, K., Evans,

N., Hollis, J., McDonald, B., and Gardiner, N. J. (2018). Apatite: a U–Pb thermochronometer or geochronometer? *Lithos*, 318, 143–157.

Klepeis, K. A., Crawford, M. L., and Gehrels, G. (1998). Structural history of the crustal-scale Coast shear zone north of Portland Canal, southeast Alaska and British Columbia. *J. Struct. Geol.*, 20(7), 883–904.

Kohn, M. J. (2016). Metamorphic chronology—a tool for all ages: Past achievements and future prospects. *Am. Mineral.*, 101(1), 25–42.

Kohn, M. J. (2020). A refined zirconium-in-rutile thermometer. *Am. Mineral. J. Earth Planet. Materials*, 105(6), 963–971.

Kohn, M. J. and Corrie, S. L. (2011). Preserved Zr-temperatures and U–Pb ages in high-grade metamorphic titanite: evidence for a static hot channel in the Himalayan orogen. *Earth Planet. Sci. Lett.*, 311(1–2), 136–143.

Kohn, M. J., Engi, M., and Lanari, P. (2017). *Petrochronology: Methods and Applications*, volume 83 of *Reviews in Mineralogy and Geochemistry*. Mineralogical Society of America.

Konrad-Schmolke, M., Zack, T., O'Brien, P. J., and Jacob, D. E. (2008). Combined thermodynamic and rare earth element modelling of garnet growth during subduction: Examples from ultrahigh-pressure eclogite of the Western Gneiss Region, Norway. *Earth Planet. Sci. Lett.*, 272(1–2), 488–498.

Korhonen, F. J., Clark, C., Brown, M., Bhattacharya, S., and Taylor, R. (2013). How long-lived is ultrahigh temperature (UHT) metamorphism? Constraints from zircon and monazite geochronology in the Eastern Ghats orogenic belt, India. *Precambrian Res.*, 234, 322–350.

Kotowski, A. J., Cisneros, M., Behr, W. M., Stockli, D. F., Soukis, K., Barnes, J. D., and Ortega-Arroyo, D. (2022). Subduction, underplating, and return flow recorded in the Cycladic Blueschist Unit exposed on Syros, Greece. *Tectonics*, 41(6), article no. e2020TC006528.

Kylander-Clark, A. R., Hacker, B. R., and Cottle, J. M. (2013). Laser-ablation split-stream ICP petrochronology. *Chem. Geol.*, 345, 99–112.

Kylander-Clark, A. R. C., Hacker, B. R., and Mattinson, J. M. (2008). Slow exhumation of UHP terranes: titanite and rutile ages of the Western Gneiss Region, Norway. *Earth Planet. Sci. Lett.*, 272(3–4), 531–540.

Labrousse, L., Duretz, T., and Gerya, T. (2015). H_2O-fluid-saturated melting of subducted continental crust facilitates exhumation of ultrahigh-pressure rocks in continental subduction zones. *Earth Planet. Sci. Lett.*, 428, 151–161.

Labrousse, L., Jolivet, L., Andersen, T. B., Agard, P., Hébert, R., Maluski, H., and Schärer, U. (2004). Pressure–temperature–time deformation history of the exhumation of ultra-high pressure rocks in the Western Gneiss Region, Norway. In *Gneiss Domes in Orogeny*, Special Papers-Geological Society of America, pages 155–184. Geological Society of America.

Lacombe, O. and Beaudoin, N. E. (2024). Timing, sequence, duration and rate of deformation in fold-and-thrust belts: a review of traditional approaches and recent advances from absolute dating (K–Ar illite/U–Pb calcite) of brittle structures. *C. R. Géosci.*, 356(S2), 467–494. (this issue).

Larson, K. P., Shrestha, S., Cottle, J. M., Guilmette, C., Johnson, T. A., Gibson, H. D., and Gervais, F. (2022). Re-evaluating monazite as a record of metamorphic reactions. *Geosci. Front.*, 13(2), article no. 101340.

Laurent, V., Huet, B., Labrousse, L., Jolivet, L., Monié, P., and Augier, R. (2017). Extraneous argon in high-pressure metamorphic rocks: Distribution, origin and transport in the Cycladic Blueschist Unit (Greece). *Lithos*, 272, 315–335.

Laurent, V., Jolivet, L., Roche, V., Augier, R., Scaillet, S., and Cardello, G. L. (2016). Strain localization in a fossilized subduction channel: Insights from the Cycladic Blueschist Unit (Syros, Greece). *Tectonophysics*, 672, 150–169.

Laurent, V., Lanari, P., Naïr, I., Augier, R., Lahfid, A., and Jolivet, L. (2018). Exhumation of eclogite and blueschist (Cyclades, Greece): Pressure–temperature evolution determined by thermobarometry and garnet equilibrium modelling. *J. Metamorph. Geol.*, 36(6), 769–798.

Laurent, V., Scaillet, S., Jolivet, L., Augier, R., and Roche, V. (2021). ^{40}Ar behaviour and exhumation dynamics in a subduction channel from multiscale ^{40}Ar/^{39}Ar systematics in phengite. *Geochim. Cosmochim. Acta*, 311, 141–173.

Logue, A. S., Bybee, G. M., Tappa, M. J., Baxter, E., and Iaccheri, L. (2022). A novel, laser-based microsampling technique for texturally controlled, combined and complementary Sr and Nd isotope measurements in silicate minerals. *Geostand. Geoanal. Res.*, 46(4), 789–809.

Lotout, C., Pitra, P., Poujol, M., Anczkiewicz, R., and Van Den Driessche, J. (2018). Timing and duration of Variscan high-pressure metamorphism in the French Massif Central: A multimethod geochronological study from the Najac Massif. *Lithos*, 308, 381–394.

Manzotti, P., Bosse, V., Pitra, P., Robyr, M., Schiavi, F., and Ballèvre, M. (2018). Exhumation rates in the Gran Paradiso Massif (Western Alps) constrained by in situ U–Th–Pb dating of accessory phases (monazite, allanite and xenotime). *Contrib. Mineral. Petrol.*, 173, 1–28.

Manzotti, P., Schiavi, F., Nosenzo, F., Pitra, P., and Ballèvre, M. (2022). A journey towards the forbidden zone: a new, cold, UHP unit in the Dora-Maira Massif (Western Alps). *Contrib. Mineral. Petrol.*, 177(6), article no. 59.

March, S., Hand, M., Tamblyn, R., Carvalho, B. B., and Clark, C. (2022). A diachronous record of metamorphism in metapelites of the Western Gneiss Region, Norway. *J. Metamorph. Geol.*, 40(6), 1121–1158.

McClelland, W. C. and Lapen, T. J. (2013). Linking time to the pressure–temperature path for ultrahigh-pressure rocks. *Elements*, 9(4), 273–279.

McClelland, W. C., Power, S. E., Gilotti, J. A., Mazdab, F. K., and Wopenka, B. (2006). U–Pb SHRIMP geochronology and trace-element geochemistry of coesite-bearing zircons, North-East Greenland Caledonides. In Hacker, B. R., McClelland, W. C., and Liou, J., editors, *Ultrahigh-Pressure Metamorphism: Deep Continental Subduction*, Special Paper of the Geological Society of America, v403. Geological Society of America, Boulder, CO.

Millonig, L. J., Albert, R., Gerdes, A., Avigad, D., and Dietsch, C. (2020). Exploring laser ablation U–Pb dating of regional metamorphic garnet–the Straits Schist, Connecticut, USA. *Earth Planet. Sci. Lett.*, 552, article no. 116589.

Miyashiro, A. (1961). Evolution of metamorphic belts. *J. Petrol.*, 2(3), 277–311.

Moser, A. C., Hacker, B. R., Gehrels, G. E., Seward, G. G., Kylander-Clark, A. R., and Garber, J. M. (2022). Linking titanite U–Pb dates to coupled deformation and dissolution–reprecipitation. *Contrib. Mineral. Petrol.*, 177(3), article no. 42.

Moser, D. E., Corfu, F., Darling, J. R., Reddy, S. M., and Tait, K., editors (2017). *Microstructural Geochronology: Planetary Records Down to Atom Scale*. John Wiley & Sons, Hoboken, NJ.

Mottram, C. M., Cottle, J. M., and Kylander-Clark, A. R. (2019). Campaign-style U–Pb titanite petrochronology: along-strike variations in timing of metamorphism in the Himalayan metamorphic core. *Geosci. Front.*, 10(3), 827–847.

Nicoli, G., Moyen, J. F., and Stevens, G. (2016). Diversity of burial rates in convergent settings decreased as Earth aged. *Sci. Rep.*, 6(1), article no. 26359.

Nicollet, C., Bosse, V., Spalla, M. I., and Schiavi, F. (2018). Eocene ultra-high temperature (UHT) metamorphism in the Gruf complex (Central Alps): constraints by LA-ICPMS zircon and monazite dating in petrographic context. *J. Geol. Soc.*, 175(5), 774–787.

Nteme, J., Scaillet, S., Brault, P., and Tassan-Got, L. (2022). Atomistic simulations of ^{40}Ar diffusion in muscovite. *Geochim. Cosmochim. Acta*, 331, 123–142.

Olierook, H. K., Taylor, R. J., Erickson, T. M., Clark, C., Reddy, S. M., Kirkland, C. L., et al. (2019). Unravelling complex geologic histories using U–Pb and trace element systematics of titanite. *Chem. Geol.*, 504, 105–122.

Oriolo, S., Schulz, B., Hueck, M., Oyhantçabal, P., Heidelbach, F., Sosa, G., et al. (2022). The petrologic and petrochronologic record of progressive vs polyphase deformation: Opening the analytical toolbox. *Earth Sci. Rev.*, 234, article no. 104235.

Palin, R. M., Santosh, M., Cao, W., Li, S. S., Hernández-Uribe, D., and Parsons, A. (2020). Secular change and the onset of plate tectonics on Earth. *Earth Sci. Rev.*, 207, article no. 103172.

Pitra, P., Poujol, M., Van Den Driessche, J., Bretagne, E., Lotout, C., and Cogné, N. (2022). Late Variscan (315 Ma) subduction or deceptive zircon REE patterns and U–Pb dates from migmatite-hosted eclogites? (Montagne Noire, France). *J. Metamorph. Geol.*, 40(1), 39–65.

Robinson, P. (1995). Extension of Trollheimen tectono-stratigraphic sequence in deep synclines near Molde and Brativag, Western Gneiss Region, southern Norway. *Norsk Geologisk Tidsskrift*, 75(4), 181–197.

Rubatto, D. (2002). Zircon trace element geochemistry: partitioning with garnet and the link between U–Pb ages and metamorphism. *Chem. Geol.*, 184(1–2), 123–138.

Rubatto, D. (2017). Zircon: the metamorphic mineral. *Rev. Mineral. Geochem.*, 83(1), 261–295.

Rubatto, D. and Hermann, J. (2001). Exhumation as fast as subduction? *Geology*, 29(1), 3–6.

Rubatto, D., Hermann, J., Berger, A., and Engi, M. (2009). Protracted fluid-induced melting during Barrovian metamorphism in the Central Alps. *Contrib. Mineral. Petrol.*, 158, 703–722.

Rubatto, D., Regis, D., Hermann, J., Boston, K., Engi, M., Beltrando, M., and McAlpine, S. R. (2011). Yo-yo subduction recorded by accessory minerals in the Italian Western Alps. *Nat. Geosci.*, 4(5), 338–342.

Ruh, J. B., Le Pourhiet, L., Agard, P., Burov, E., and Gerya, T. (2015). Tectonic slicing of subducting oceanic crust along plate interfaces: Numerical modeling. *Geochem. Geophys. Geosyst.*, 16(10), 3505–3531.

Schaltegger, U., Fanning, C. M., Günther, D., Maurin, J. C., Schulmann, K., and Gebauer, D. (1999). Growth, annealing and recrystallization of zircon and preservation of monazite in high-grade metamorphism: conventional and in-situ U–Pb isotope, cathodoluminescence and microchemical evidence. *Contrib. Mineral. Petrol.*, 134, 186–201.

Schaltegger, U., Schmitt, A. K., and Horstwood, M. S. A. (2015). U–Th–Pb zircon geochronology by ID-TIMS, SIMS, and laser ablation ICP-MS: Recipes, interpretations, and opportunities. *Chem. Geol.*, 402, 89–110.

Schärer, U. and Labrousse, L. (2003). Dating the exhumation of UHP rocks and associated crustal melting in the Norwegian Caledonides. *Contrib. Mineral. Petrol.*, 144, 758–770.

Scherer, E., Munker, C., and Mezger, K. (2001). Calibration of the lutetium-hafnium clock. *Science*, 293(5530), 683–687.

Schoene, B. (2014). 4.10-U–Th–Pb Geochronology. *Treatise Geochem.*, 4, 341–378.

Schulz, B. (2021). Monazite microstructures and their interpretation in petrochronology. *Front. Earth Sci.*, 9, article no. 668566.

Schulz, B. and Krause, J. (2018). Petrochronology of kinzigites in the Variscan Saxonian Granulite Massif by electron microprobe analysis and electron microscopy. *GeoBonn*, 2018, article no. A-241. Abstracts-A.

Schumacher, J. C., Brady, J. B., and Cheney, J. T. (2008). Metamorphic style and development of the blueschist-to eclogite-facies rocks, Cyclades, Greece. In *IOP Conference Series: Earth and Environmental Science*, volume 2, no. 1, page 012017. IOP Publishing, Bristol.

Seydoux-Guillaume, A. M., Fougerouse, D., Laurent, A. T., Gardés, E., Reddy, S. M., and Saxey, D. W. (2019). Nanoscale resetting of the Th/Pb system in an isotopically-closed monazite grain: A combined atom probe and transmission electron microscopy study. *Geosci. Front.*, 10(1), 65–76.

Simpson, A., Gilbert, S., Tamblyn, R., Hand, M., Spandler, C., Gillespie, J., et al. (2021). In-situ Lu-Hf geochronology of garnet, apatite and xenotime by LA ICP MS/MS. *Chem. Geol.*, 577, article no. 120299.

Smit, M. A., Scherer, E. E., and Mezger, K. (2013). Lu–Hf and Sm–Nd garnet geochronology: chronometric closure and implications for dating petrological processes. *Earth Planet. Sci. Lett.*, 381, 222–233.

Sobolev, S. V. and Brown, M. (2019). Surface erosion events controlled the evolution of plate tectonics on Earth. *Nature*, 570(7759), 52–57.

Söderlund, U., Patchett, P. J., Vervoort, J. D., and Isachsen, C. E. (2004). The ^{176}Lu decay constant determined by Lu–Hf and U–Pb isotope systematics of Precambrian mafic intrusions. *Earth Planet. Sci. Lett.*, 219(3–4), 311–324.

Soret, M., Bonnet, G., Agard, P., Larson, K. P., Cottle, J. M., Dubacq, B., et al. (2022). Timescales of subduction initiation and evolution of subduction thermal regimes. *Earth Planet. Sci. Lett.*, 584, article no. 117521.

Spear, F. S. and Pyle, J. M. (2010). Theoretical modeling of monazite growth in a low-Ca metapelite. *Chem. Geol.*, 273(1–2), 111–119.

Spencer, K. J., Hacker, B. R., Kylander-Clark, A. R. C., Andersen, T. B., Cottle, J. M., Stearns, M. A., et al. (2013). Campaign-style titanite U–Pb dating by laser-ablation ICP: Implications for crustal flow, phase transformations and titanite closure. *Chem. Geol.*, 341, 84–101.

Stern, R. J. (2005). Evidence from ophiolites, blueschists, and ultrahigh-pressure metamorphic terranes that the modern episode of subduction tectonics began in Neoproterozoic time. *Geology*, 33(7), 557–560.

Tamblyn, R., Hand, M., Simpson, A., Gilbert, S., Wade, B., and Glorie, S. (2022). In situ laser ablation Lu–Hf geochronology of garnet across the Western Gneiss Region: campaign-style dating of metamorphism. *J. Geol. Soc.*, 179(4), article no. jgs2021-094.

Taylor, R. J., Kirkland, C. L., and Clark, C. (2016). Accessories after the facts: Constraining the timing, duration and conditions of high-temperature metamorphic processes. *Lithos*, 264, 239–257.

Tettelaar, T. and Indares, A. (2007). Granulite-facies regional and contact metamorphism of the Tasiuyak paragneiss, northern Labrador: textural evolution and interpretation. *Can. J. Earth Sci.*, 44(10), 1413–1437.

Tillberg, M., Drake, H., Zack, T., Kooijman, E., Whitehouse, M. J., and Åström, M. E. (2020). In situ Rb–Sr dating of slickenfibres in deep crystalline basement faults. *Sci. Rep.*, 10(1), 1–13.

Tilton, G. R., Patterson, C., Brown, H., Inghram, M., Hayden, R., Hess, D., and Larsen Jr, E. (1955). sotopic composition and distribution of lead, uranium, and thorium in a Precambrian granite. *Geol. Soc. Am. Bull.*, 66(9), 1131–1148.

Timms, N. E., Kinny, P. D., Reddy, S. M., Evans, K., Clark, C., and Healy, D. (2011). Relationship among titanium, rare earth elements, U–Pb ages and deformation microstructures in zircon: Implications for Ti-in-zircon thermometry. *Chem. Geol.*, 280(1–2), 33–46.

Tomkins, H. S., Powell, R., and Ellis, D. J. (2007). The pressure dependence of the zirconium-in-rutile thermometer. *J. Metamorph. Geol.*, 25(6), 703–713.

Trotet, F., Jolivet, L., and Vidal, O. (2001). Tectono-metamorphic evolution of Syros and Sifnos islands (Cyclades, Greece). *Tectonophysics*, 338(2), 179–206.

Tual, L., Smit, M. A., Cutts, J., Kooijman, E., Kielman-Schmitt, M., Majka, J., and Foulds, I. (2022). Rapid, paced metamorphism of blueschists (Syros, Greece) from laser-based zoned Lu-Hf garnet chronology and LA-ICPMS trace element mapping. *Chem. Geol.*, 607, article no. 121003.

Umhoefer, P. J., Whitney, D. L., Teyssier, C., Fayon, A. K., Casale, G., and Heizler, M. T. (2007). Yo-yo tectonics in a wrench zone, Central Anatolian fault zone, Turkey. In Roeske, S. M., Till, A. B., Foster, D. A., and Sample, J. C., editors, *Exhumation Associated with Continental Strike-Slip Fault Systems*, Special Paper of the Geological Society of America, v434. Geological Society of America, Boulder, CO.

Uunk, B., Brouwer, F., de Paz-Álvarez, M., van Zuilen, K., Huybens, R., van't Veer, R., and Wijbrans, J. (2022). Consistent detachment of supracrustal rocks from a fixed subduction depth in the Cyclades. *Earth Planet. Sci. Lett.*, 584, article no. 117479.

Viete, D. R., Kylander-Clark, A. R., and Hacker, B. R. (2015). Single-shot laser ablation split stream (SS-LASS) petrochronology deciphers multiple, short-duration metamorphic events. *Chem. Geol.*, 415, 70–86.

Viete, D. R. and Lister, G. S. (2017). On the significance of short-duration regional metamorphism. *J. Geol. Soc.*, 174(3), 377–392.

Villa, I. M. (1998). Isotopic closure. *Terra Nova*, 10, 42–47.

Villa, I. M. (2016). Diffusion in mineral geochronometers: present and absent. *Chem. Geol.*, 420, 1–10.

Walczak, K., Barnes, C. J., Majka, J., Gee, D. G., and Klonowska, I. (2022). Zircon age depth-profiling sheds light on the early Caledonian evolution of the Seve Nappe Complex in west-central Jämtland. *Geosci. Front.*, 13(2), article no. 101112.

Watson, E. B., Wark, D. A., and Thomas, J. B. (2006). Crystallization thermometers for zircon and rutile. *Contrib. Mineral. Petrol.*, 151(4), 413–433.

Weinberg, R. F., Wolfram, L. C., Nebel, O., Hasalová, P., Závada, P., Kylander-Clark, A. R., and Becchio, R. (2020). Decoupled U–Pb date and chemical zonation of monazite in migmatites: The case for disturbance of isotopic systematics by coupled dissolution-reprecipitation. *Geochim. Cosmochim. Acta*, 269, 398–412.

White, R. W., Powell, R., and Holland, T. J. B. (2007). Progress relating to calculation of partial melting equilibria for metapelites. *J. Metamorph. Geol.*, 25(5), 511–527.

Wiest, J. D., Jacobs, J., Fossen, H., Ganerød, M., and Osmundsen, P. T. (2021). Segmentation of the Caledonian orogenic infrastructure and exhumation of the Western Gneiss Region during transtensional collapse. *J. Geol. Soc.*, 178(3), article no. jgs2020-199.

Wijbrans, J. R., Schliestedt, M., and York, D. (1990). Single grain argon laser probe dating of phengites from the blueschist to greenschist transition on Sifnos (Cyclades, Greece). *Contrib. Mineral. Petrol.*, 104, 582–593.

Willigers, B. J. A., Van Gool, J. A. M., Wijbrans, J. R., Krogstad, E. J., and Mezger, K. (2002). Post-tectonic cooling of the Nagssugtoqidian orogen and a comparison of contrasting cooling histories in Precam-

brian and Phanerozoic orogens. *J. Geol.*, 110(5), 503–517.

Yakymchuk, C. and Brown, M. (2014). Behavior of zircon and monazite during crustal melting. *J. Geol. Soc.*, 171(4), 465–479.

Yamato, P. and Brun, J. P. (2017). Metamorphic record of catastrophic pressure drops in subduction zones. *Nat. Geosci.*, 10(1), 46–50.

York, D. (1966). Least-squares fitting of a straight line. *Can. J. Phys.*, 44(5), 1079–1086.

Young, D. J. (2018). Structure of the (ultra) high-pressure Western Gneiss Region, Norway: Imbrication during Caledonian continental margin subduction. *GSA Bull.*, 130(5–6), 926–940.

Zack, T. and Hogmalm, K. J. (2016). Laser ablation Rb/Sr dating by online chemical separation of Rb and Sr in an oxygen-filled reaction cell. *Chem. Geol.*, 437, 120–133.

Zack, T., Moraes, R. D., and Kronz, A. (2004). Temperature dependence of Zr in rutile: empirical calibration of a rutile thermometer. *Contrib. Mineral. Petrol.*, 148, 471–488.